The financial cost of stabilizing US farm income under climate change

Cécile Couharde, Rémi Generoso

The financial cost of stabilizing US farm income under climate change

Cécile Couharde
Rémi Generoso

2023-18 Document de Travail/ Working Paper

EconomiX - UMR 7235 Bâtiment Maurice Allais
Université Paris Nanterre 200, Avenue de la République
92001 Nanterre Cedex

Site Web : economix.fr
Contact : secreteriat@economix.fr
Twitter : @EconomixU

The financial cost of stabilizing US farm income under climate change*

Cécile Couharde[a], Rémi Generoso[b,*]

[a] *EconomiX-CNRS, University Paris Nanterre*
[b] *LEM-CNRS, University of Lille*

Abstract

The paper assesses the financial cost of federal farm programs in mitigating income losses due to drier conditions expected from climate change. Our study encompasses agricultural-producing counties within the conterminous United States during the census years from 2002 to 2017. We quantify historical drought patterns and their projected trends for the near (2020-2049) and more distant (2030-2059) future, using climate reanalysis data and 20 downscaled global circulation model products from the Coupled Model Intercomparison Project 5. We estimate the relationship between federal agricultural payments and climate change by analyzing how farm income losses due to drier conditions affect the magnitude and distribution of these payments under the RCP 8.5 scenario. We predict that, under unmitigated climate change, payments from federal farm program should significantly increase to maintain their income–stabilization capacity, with a greater likelihood of much larger financial costs when accounting for statistical and climate uncertainties.

Keywords: `Climate change, Farm income, Federal farm payments, Uncertainty`

*The authors thank conference participants at the 2022 Canadian Economic Association Annual Congress (held at Polytechnique Montréal, May 11-13th) for their helpful comments.

*Corresponding author. LEM UMR 9221, Université de Lille, Bâtiment SH2 Cité scientifique, 59650 Villeneuve d'Ascq, France. Email:`remi.generoso@univ-lille.fr`

1. Introduction

Among the potential realizations of climate change, droughts are expected to present a growing threat to American agriculture in the coming decades, as their frequency and severity across the United States are projected to increase with climate change (Ahmadalipour et al., 2017; Wuebbles et al., 2017; Pörtner et al., 2022). While many economic studies have examined the impact of future droughts on crop yields and farm incomes (Deschênes and Greenstone, 2007; Schlenker and Roberts, 2009; Tack et al., 2015; Burke and Emerick, 2016; Rodziewicz and Dice, 2020), less consideration has been given to their financial implications on payments from federal farm programs. Yet, these subsidy programs are still primary mechanisms that protect farmers' incomes from changes in weather, market prices, and other factors that can affect agricultural production and profitability. Therefore, it is likely that drier conditions expected from climate change will have a significant effect on the costs of these farm programs, particularly if their existing structure is maintained.

In this paper, we estimate the capacity of federal payment programs to smooth farm income in the face of drier conditions across the Conterminous United States (CONUS) and major commodity crops and use these estimates to predict the financial cost of stabilizing farm income under climate change. We specifically focus on the near (2020–2049) and more distant (2030–2059) future climate projections made under the Representative Concentration Pathway 8.5 (RCP 8.5), the highest emissions pathway used in Intergovernmental Panel on Climate Change (IPCC) scenarios.[1] We select this future warming scenario, as it is in close agreement with historical total cumulative CO2 emissions, and is also the best match out to mid-century under current and stated policies with still highly plausible levels of CO2 emissions in 2100 (Reidmiller et al., 2018; Schwalm et al., 2020).

Our analysis proceeds in three parts. First, we assemble a panel dataset from the United States Department of Agriculture (USDA) covering agricultural–producing counties over the CONUS from the census years 2002 to 2017. We calculate farm income by taking the difference between total agricultural sales receipts (excluding federal payments) and total production costs at the county level. We only consider income support payments from federal programs that are designed to provide payments to farmers when they face unfavorable production or market conditions. We combine these data with measures of water availability during the crop growing season based on the Standardized Precipitation Evapotranspiration Index (SPEI). We then conduct parametric and non–parametric estimations to determine the capacity of income support payments to smooth income losses caused by drought conditions across the CONUS and major commodity crops. Because our main hypothesized channel linking droughts to payments from federal farm programs operates through losses

[1] This scenario corresponds to a temperature increase of about 4.3°C by 2100, compared to pre–industrial temperatures.

in agricultural incomes, we employ an instrumental variables method, which allows us to account for endogeneity bias and to estimate an accurate income–stabilizing rate. Our findings show that income support payments partly offset income losses due to drought events during the observed period (2002–2017), with a heterogeneous degree among crop categories. These results are robust to an alternative drought index, a set of controls, and a placebo test. Additionally, the bootstrap results indicate that our mean estimates provide an unbiased benchmark for assessing the potential impacts of climate change. Finally, armed with this empirical evidence, we perform a counterfactual empirical exercise to project the financial costs of stabilizing farm incomes for the CONUS and major commodity crops under expected climate change. We calculate these costs at the county–level by combining our mean estimates with projected shifts in the future drought distribution for each county based on 20 global circulation models (GCMs) and a multi–model ensemble average. This allows us to predict both the cost impact of climate change and its associated uncertainty and to characterize the inter-county variation of such impact. We find that long–run trends in climate would have a significant effect on income support payments. Our point estimates combined with climate projections from a multi-model ensemble average suggest that income support payments could reach an average of $US 116 (in 2011 prices) per operation with drought conditions projected for the period 2030–2059, compared to $US 55 (in 2011 prices) per operation over the studied period (2002–2017). When accounting for statistical and climate model uncertainties, this increase would be even higher, bringing income support payments to an average of around $US 130 (in 2011 prices) per operation. Despite an expected decrease in their contribution to the total cost, agricultural areas producing corn and soybeans should still account for over 46% of total income support payments. These findings must best be interpreted as providing a plausible benchmark on what the mid-term cost of stabilizing farm incomes under unmitigated climate change could be, given current US agricultural policy and farmers' strategies.[2]

Our paper is related to two strands of literature. The first one seeks to evaluate drought-induced costs under global warming by quantifying their financial implications on federal government supports for agriculture. The second strand of literature aims to assess the impact of climate change on agricultural outcomes by adopting a panel data method (see Blanc and Schlenker (2017) for an overview). We adopt a similar approach, acknowledging with this literature that the panel approach with fixed effects controls for unobservable time–invariant factors across regions and better addresses the omitted variable problem compared to other approaches (Deschênes and Greenstone, 2007).

[2]The empirical evidence on adaptation in US agriculture is mixed. Butler and Huybers (2013) demonstrated maize being locally adapted to hot temperatures in US counties, while Roberts and Schlenker (2011) found that corn and soybean yields had become more sensitive to extreme heat. Keane and Neal (2020) found significant adaptation occurring across hot/cool counties and over time from 1950 to 1989. However, Burke and Emerick (2016) found limited evidence for adaptation when exploiting large variations in recent temperature and precipitation trends.

Our work expands on these studies in two primary ways. First, by focusing on agricultural subsidies to farmers in response to adverse conditions, we complement studies that have typically examined the climate change effects on subsidized insurance provided by the Federal Crop Insurance Program (Crane-Droesch et al., 2019). Even though agricultural risk management has become more important over time within the Farm bill, income support payments to farmers in response to adverse production or market conditions remain a core component of US agricultural policy. Therefore, the risk of larger drought-related income losses due to climate change raises the critical questions of how much income support payments should be increased to maintain their income-stabilization capacity and how this financial cost could be mitigated, given that the additional funds needed to maintain this objective under global warming could significantly burden public finances in the coming decades.

Second, we account for the uncertainties associated with the assessment of climate change effects. We utilize high temporal and spatial resolution data on projected precipitation, temperature, soil moisture, or evapotranspiration from existing downscaled daily climate projections covering the CONUS to more accurately characterize future drought conditions and how the cost of mitigating drought-induced farm income losses varies with local climate. We employ a non-parametric bootstrap approach to handle the uncertainty surrounding our mean estimates. Mean values inferred from skewed cost distribution with parametric methods may not reflect the real costs of stabilizing farm income. It is thus essential to provide confidence intervals of cost estimates in order to reduce forecast bias. We also tackle the uncertainties associated with GCMs, as the skill of the models in representing historical droughts is very varied and leads to significant discrepancies in drought projections across models. The consensus across climate studies is that multiple GCMs and an ensemble of downscaling methods that include bias correction should be employed to ensure that the full range of possible outcomes is explored and accounted for (Knutti et al., 2010). However, a wide range of studies assessing the economic impacts of climate change uses only a single or a few models, leading to potentially misleading projections (Burke et al., 2015). To overcome these limitations and improve the accuracy of our representation of the climate system, we utilize an ensemble of GCMs to account for their inherent uncertainty. Considering statistical and climate model uncertainties provides a more accurate assessment of the possible range of projected costs of stabilizing farm incomes under climate change and ultimately helps improve decision-making in agricultural management.[3]

[3]We do not address the uncertainty caused by unexpected future for radiative forcings by using a single emissions scenario (the RCP 8.5 scenario). Hawkins and Sutton (2009) argue that this uncertainty is of relatively minor significance until the mid-twenty-first century, while becoming more significant at the end of the century. We also ignore other sources of uncertainty derived from natural fluctuations (e.g., the El Niño/Southern Oscillation (ENSO), the thermohaline–driven oceanic circulation, and the existing heat content in oceans) and the imperfect structure of downscaling methods.

The remainder of the paper is organized as follows. In Section 2, we detail the framework to quantify present and future drought conditions, which combines real-time weather data and global circulation model forecasts. We then document in Section 3 our dataset and our econometric method to link drought, agricultural income, and income support payments. In Section 4, we present our main results for the CONUS and by main commodity crops, and detail the statistical uncertainty surrounding our estimates based on historical data. Section 5 uses data from global circulation models to build projections of income support payments under climate change, considering the statistical uncertainty of our point estimates and the uncertainty associated with climate model projections. Section 6 concludes.

2. Quantifying current and future droughts: methodology and data

We gather weather data to assess the impact of local climate on US agriculture and utilize Global Circulation Model (GCM) outputs to predict its future effect under climate change. To minimize measurement errors, we follow the recommendations from Auffhammer et al. (2013) and Burke et al. (2015). Our data includes high-resolution (4-km grid cells) climate data, which reduces uncertainties in climate simulations across the CONUS, and an ensemble of 20 GCM climate projections from the Intergovernmental Panel on Climate Change (IPCC) Coupled Model Intercomparison Project 5 (CMIP5) to increase confidence in drought event predictions.

2.1. Weather variables and climate uncertainties

We rely on reanalysis products to estimate the impact of local climate on US agriculture. Compared to traditional station-based data, these products provide consistent historical records of numerous meteorological variables spanning the globe at various spatial and temporal resolutions. We download meteorological variables from the Gridded Surface Meteorological (gridMET) dataset.[4] This source provides daily high-spatial resolution (4-km) gridded surface meteorological data, such as temperature, precipitation, wind speed, relative humidity, and solar radiation, among others, that covers the CONUS from 1979 to the present. The gridMET dataset combines satellite and weather station data to provide accurate climate information (see Abatzoglou (2013) for a complete description of the dataset). It has been widely used in applications such as drought monitoring, crop yield forecasting, and water resource management due to its ability to accurately reproduce observed climate variability and extreme events in the CONUS (Blankenau et al., 2020).

The evaluation of the expected effects of climate change relies on predictions of how relevant climate variables will change in the future. In the climate impacts literature, it is common to get future values of climate variables from predictions of GCMs, based on different Representative Concentration

[4] https://www.northwestknowledge.net/metdata/data/

Pathways (RCP) scenarios. However, GCMs have a coarse spatial resolution, which can limit their ability to accurately reflect regional or local–scale climate features and processes, particularly in areas with complex topography or small–scale weather patterns. To improve the spatial resolution of GCM data, statistical or dynamical downscaling methods can be used, although these methods can add further sources of uncertainty (Auffhammer et al., 2013).

Several datasets on climate projections for North America, publicly available for download, include climate variables that are downscaled to different grid resolutions (see Kim et al. (2022) for a comparison of datasets for the CONUS). We get projections of climate variables over the CONUS from the MACA v2 dataset, which is accessible at `https://climate.nortwestknowledge.net/MACA/`. This dataset contains data from various GCMs of the Coupled Model Intercomparison Project CMIP5, which have been downscaled using the Multivariate Adaptive Constructed Analogs (MACA) approach.[5] The MACA v2 dataset provides high-resolution (4 km) daily climate projections for the CONUS. This dataset is especially useful for analyzing the regional or local impacts of climate change, such as on water resource management or agriculture, as it provides high–resolution climate projections tailored for the United States. Another advantage of the MACA database is that it offers a set of comparable model simulations derived from 20 downscaled GCMs (out of the 23 CMIP5 GCMs) gathered into a Multi–Model Ensemble (MME).[6] As no single model can adequately describe the overall process of climate systems, relying on multiple downscaled GCMs into a MME provides a more robust solution by generating climate forecasts based on a set of model ensembles.

We obtain our climate projections by calculating an unweighted MME average, which assigns the same weight to each climate model. This approach is preferred because it avoids subjective weighting or selection criteria, thus increasing the reliability of climate projections. Additionally, an unweighted MME average can be more robust to outliers and biases in individual models than weighted schemes. Even, weighted schemes assigning more weight to models that perform well in historical simulations can lead to overconfidence in their future projections, as they may not capture the full range of uncertainty. An unweighted approach avoids this potential bias and provides a more comprehensive view of the range of possible outcomes (Houghton et al., 2001). However, since the best way to handle multiple GCM projections remains a controversial issue, we perform several tests in Appendix A to compare the performance of the MME average to the 20 GCMs. The performance metrics clearly indicate that the MME average outperforms any individual model in its ability to reproduce observed weather patterns. This result is consistent with the MME benefits found in other multi–model ensemble studies (Peng et al., 2002; Kharin and Zwiers, 2002; Tebaldi

[5] More details of this statistical downscaling method can be found in Abatzoglou (2013).
[6] See Table A.1 in Appendix A for a description of the 20 downscaled GCMs in the MACA v2 dataset.

and Knutti, 2007).

To account for the uncertainty due to multiple projections from different GCMs, we also compare the projections from the MME average to those from individual GCMs, without assigning any weighting to the individual GCMs and independently of their relative performance to characterize the past climate at the scale of the CONUS. Figures 1.A to 1.C give a first impression of the range of projected precipitation and temperature anomalies across the 20 downscaled GCMs. These anomalies are calculated as deviations from their average over the reference period of 1950–2100.

Figure 1: *Range of projected precipitation and temperature anomalies around the multi–model ensemble average from 1950 to 2100, according to 20 MACA v2 downscaled GCMs and under the RCP 8.5 scenario*

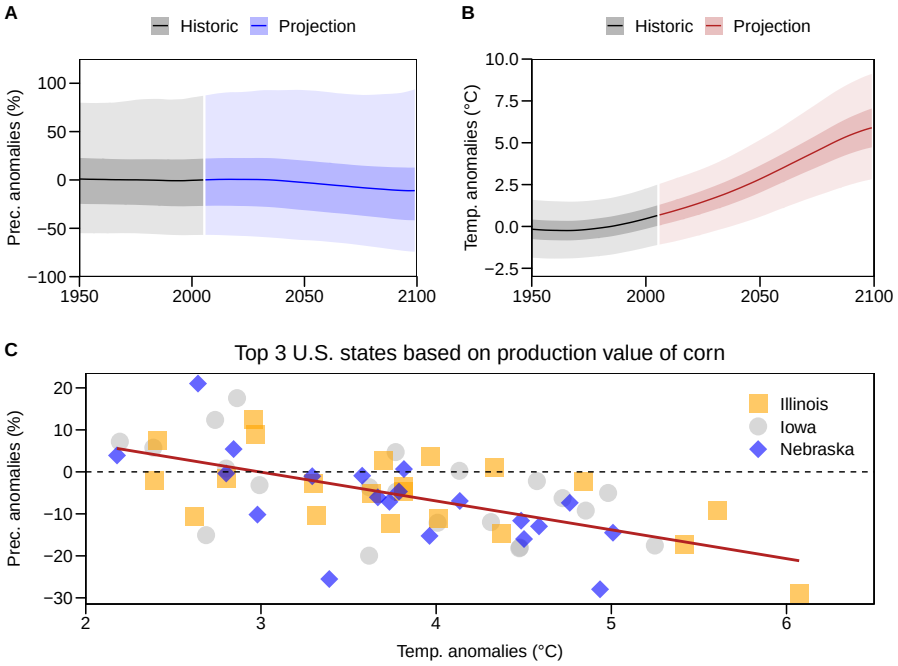

Note: Figures 1.A and 1.B illustrate the range of projected precipitation and temperature anomalies across the 20 different GCMs from the MACA v2 dataset (shaded areas) and around the multi-model ensemble average (solid lines) from 1950 to 2100 over the CONUS. Figure 1.C shows the projected precipitation and temperature anomalies from 1950 to 2100 for the top three corn producing states. These projections are also based on the 20 different GCMs from the MACA v2 dataset and compared to their central tendency (red line).

The figures reveal significant uncertainty among the predictions from the different models, especially for near–term projections and for variables with a low signal-to-noise ratio, such as precipitation.[7]

[7]Projecting changes in precipitation in a warmer climate is more complex because of uncertainty in projecting changes in the large-scale circulation that plays an essential role in the formation of clouds and precipitation (Shep-

This divergence in temperature and precipitation anomalies is also evident spatially. As shown in Figure 1.C, there is a high level of disagreement on the future climate of the top 3 corn-producing states among climate models and against their central tendency. These figures make it clear that it is not appropriate to rely on a single or just a few GCMs when estimating the impacts of climate change. Instead, all climate model outputs must be considered.

2.2. Quantifying past and future droughts

Many different drought indices have been developed, but their use has revealed several issues that have led to the development of improved formulations. Firstly, it is commonly accepted that drought indices must include precipitation in combination with other hydroclimatic variables (Mishra and Singh, 2010). The inclusion of evapotranspiration is often considered an accurate way to capture the multivariate nature of drought, along with the importance of incorporating temperature in drought analysis (Vicente-Serrano et al., 2010). Secondly, the literature places particular emphasis on standardized indices due to their ability to enable spatial and temporal comparisons, which is essential for accurate drought analysis (Vicente-Serrano et al., 2010). Lastly, using a multi–scalar index is also central, as it allows for determining the rarity and severity of drought events at any time scale of interest (McKee et al., 1995).

The Standardized Precipitation Evapotranspiration Index (SPEI) developed by Vicente-Serrano et al. (2010) is a drought index that meets these three criteria. It has been widely used in recent years to evaluate drought patterns and their impacts on agriculture in the United States (Zipper et al., 2016; Krakauer et al., 2019; Lu et al., 2020; Barai et al., 2021; Yaddanapudi and Mishra, 2022). Moreover, the literature has shown that this index has a higher capability than other drought indices to capture drought impacts on a wide variety of crops and for a wide range of periods in the south-central United States (Tian et al., 2018) and across the entire CONUS (Peña-Gallardo et al., 2019). Therefore, we use this index in this study to measure drought severity and its future changes under global warming over the CONUS.

The SPEI uses, as its input, a climatic water balance, defined as the difference between precipitation and reference evapotranspiration.[8] The method for deriving historical SPEI from the water balance series involves three steps (see Vicente-Serrano et al. (2010); Beguería et al. (2014)). First, water balance series are accumulated at a chosen time scale (3, 6, or 12–months). Second, the accumulated water balances at each grid cell are normalized by fitting them to a log-logistic probability distribution. Finally, the SPEI values are obtained as the standardized values of the probabil-

herd, 2014). Furthermore, the CONUS is located between high–latitude regions, generally projected to become wetter and the subtropical zone projected to become drier. There is, therefore, significant uncertainty about the sign and magnitude of future anthropogenic changes to seasonal precipitation in a large part of the country.

[8] See Appendix B for the definition of reference evapotranspiration.

ity distribution function of the accumulated water balance series, following the approximation of Abramowitz and Stegun (1964). This standardization process ensures that the long–term mean of the SPEI for each grid cell is zero and its variance is one. The long–term mean represents what can be considered typical climate or normal weather conditions during a fixed and common reference period. The current values of the SPEI are measured in standard deviation units and represent weather anomalies relative to the reference period, which are comparable across space and time. Negative values indicate drier conditions than the typical climate, while positive values denote wetness in excess of normal conditions.

We provide a summary of the essential steps for the SPEI assessment.[9] In this study, we choose a 3–month accumulation period to calculate the SPEI, as it is the most suitable time scale to detect drought effects on crop yields (Peña-Gallardo et al., 2019; Santini et al., 2022). We calculate reference evapotranspiration using the American Society of Civil Engineers (ASCE) Penman–Monteith formulation, as recommanded by the United Nations Food and Agriculture Organization (Allen et al., 2006). We fit the historical accumulated water balances using maximum likelihood estimation and normalize the resulting SPEI values using a three–parameter log–logistic probability distribution, relative to the climate normals based on a reference period from 1979 to 2020. This period of more than 30 consecutive years is long enough to accurately measure normal weather conditions and associated weather anomalies.

To assess future climate conditions, we compute monthly accumulated climate balance series from 1979 to 2100 for each downscaled GCM. We derive the climate balance series using a MME approach by averaging the simulated reference evapotranspiration and precipitation from all models and then calculating the difference between these two averaged series. Future SPEI values are then calibrated with the parameters of the log–logistic distribution estimated from the SPEI series computed over the reference period. This method allows the derivation of predicted changes in the mean and the variance of future SPEI while preserving their historical distribution. Consequently, the predicted SPEI will capture the overall shift caused by climate change. We forecast SPEI values and derive future weather anomalies relative to the 1979-2020 reference period for two consecutive 30–year periods corresponding to a near (2020–2049) and more distant (2030–2059) future. These two 30–year time horizons provide a suitable window for climate risk planning and accurate climate forecasts. They correspond to a MME average temperature increase of +2°C and +2.5°C above the pre–industrial level under the RCP 8.5 scenario.

Since we are interested in the effects of drought on agricultural outcomes, we compute county–level historical and future SPEI that reflect drought severity in agricultural areas. To do this, we match each SPEI grid cell value to agriculture production areas using the USDA's Cropland Data Layer

[9]The method for calculating the SPEI is detailed in Appendix B.

(CDL) hosted on CropScape.[10] The CDL is an annual crop–specific land cover map produced from satellite imagery with a resolution of 30m. It is used to determine which crops are being grown in specific areas and assess patterns and trends in crop production across the CONUS. Since the CDL is only available for limited states from 1997 to 2007, we assign the CDL data for the year 2008 to the previous SPEI values to ensure that data are comparable across counties and over time.[11] We exclude counties with low and sparse agricultural lands (cropland or pasture/hay) based on CDL counts of less than 10,000 acres (approximately 40 km^2). This leaves us with 137 counties with no agricultural land pixels, accounting for 4.4% of the counties in the CONUS. Since the CDL and SPEI datasets have different spatial resolutions, we compute an intermediate logical layer (w_i), taking the value 1 if at least one parcel is observed within each SPEI data grid i and a missing value otherwise.[12] We then spatially aggregate monthly SPEI grid cell values at the county level. We use a weighted spatial mean that considers the fraction of the cell covered by each county's borders, to obtain agricultural county-specific measures of relevant climate conditions. Finally, our analysis focuses on the crop-growing season, typically from April to November, when climatic conditions have the greatest impact on agricultural production.[13] Yearly SPEI values are therefore computed by averaging the 3–month SPEI monthly values over the crop growing season:

$$Dry_{c,t} = \frac{1}{8}\sum_{m=4}^{11}\left[\frac{1}{I_c}\left(\sum_{i=1}^{I_c} w_{i,t} \times -SPEI_{i,m}\right)\right] \tag{1}$$

Where I_c is the number of cells included in the county c.

For readability, $Dry_{c,t}$ is computed in equation 1 using the opposite values of the SPEI, so that positive values of $Dry_{c,t}$ indicate drier–than–normal conditions experienced in agricultural areas of a county c during the crop-growing season of a year t. As such, a positive coefficient related to this variable, when included as an explanatory variable in a regression, can be interpreted as the effect of a 1 standard deviation increase in drought severity from the long–term mean occurring in the agricultural areas of a county. The future climate is projected to be drier or wetter than the climate of the reference period (1979–2020), depending on whether the projected values of $Dry_{c,t}$ are positive or negative.

Maps A and B in Figure 2 show the geographical distribution of projected weather anomalies

[10] https://data.nal.usda.gov/dataset/cropscape-cropland-data-layer

[11] As generally acknowledged, the CDL is able to accurately identify major commodity crops, such as corn and soybeans. However, some minor crops, such as alfalfa, may be incorrectly categorized as non-cultivated due to their spectral similarity to non-cropland covers. According to Lark et al. (2021), specific classes can be aggregated into broader landcover domains such as cropland or non-cropland to accommodate low accuracies.

[12] The maps in Figure A.2 (Appendix A) show the geographical distribution of the layers w_i for the years 2008, 2012, and 2017.

[13] Refer to Appendix A, Figure A.3 to view the crop calendars for the United States.

relative to the 1979–2020 reference period, based on the MME average over the CONUS. Drier–than–normal conditions are projected to increase over the entire CONUS in both forecast horizons, with droughts expected to be more severe in the distant future (2030–2059) than in the near future (2020–2049). At the regional scale, most states should experience overall warming over both periods, but the severity of projected drought conditions would vary due to regional-specific climates and aridity conditions. The most significant changes are expected to occur in the western United States, where the drought index could increase by more than 0.4, which is significant, given the thresholds of 1.0, 1.5, and 2.0 representing moderate, severe, and extreme drought conditions, respectively. In contrast, New England should be the least exposed region to drier conditions. The Heartland region should also experience drought conditions, although to a lesser extent than the western United States. These findings are in line with the projections made by Ahmadalipour et al. (2017). According to these authors, climate change may lead to a considerable aggravation in the severity and extent of future droughts in the western United States, and a tendency toward more frequent and intense summer droughts across the CONUS.

Figure 2: *Future severity of droughts (as deviations from the reference period of 1979–2020) for the near (2020–2049) and more distant (2030–2059) future, under the RCP 8.5 scenario, multi–model ensemble average*

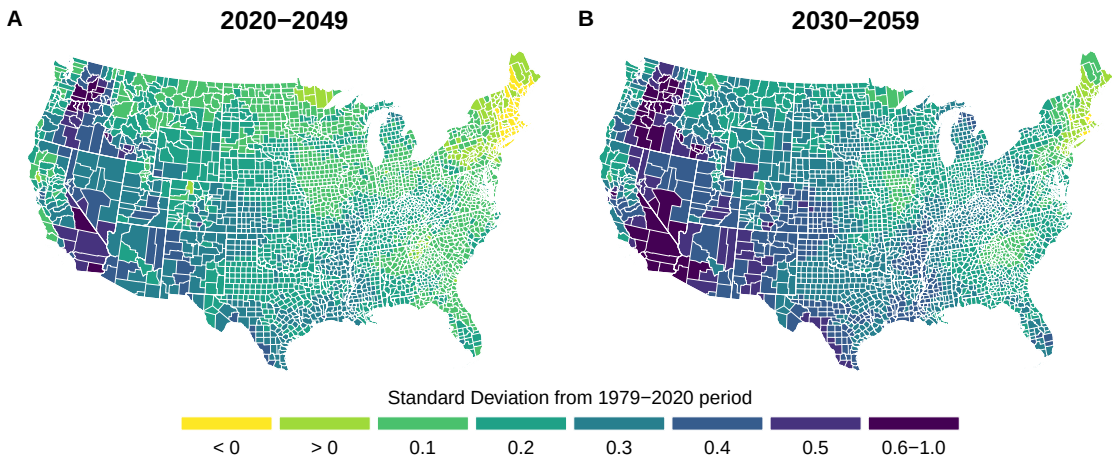

Note: Projected deviations in drought severity under the RCP 8.5 scenario across the CONUS over the near (2020–2049) and more distant (2030–2059) future, using 1979–2020 as the reference period. The drought index is based on SPEI computed at 3–month time scale and is calculated using the multi-model ensemble average. A positive value indicates an increasing value of the drought index and more severe future droughts.

While climate change is expected to intensify drought conditions over the CONUS, the exact magnitude of this intensification remains uncertain due to differences in projections among the 20 GCMs. Figure 3 shows that future SPEI are projected to increase more under several models, especially the Hadley Models (HadG–EM2–ES and HadGEM2–CC), compared to the MME average, indicating

an expected exposure of the CONUS to more severe drought events. In contrast, models such as the Geophysical Fluid Dynamics Laboratory (GDLF–ESM2G, GDFL–ESMEM) and the Meteorological Research Institute of Japan (MRI–CGM3) project smaller or unchanged drier conditions. The full range of projected SPEI over the CONUS spans from -0.03 (+0.04) to +0.56 (+0.70) for the near (more distant) future, indicating significant climate model uncertainty.

Therefore, relying on the MME average can provide a more reliable estimate of future climate conditions, as it helps to smooth out the idiosyncrasies of individual models. However, it is also important to consider the full range of model predictions to get a comprehensive view of possible future drought conditions and assess the uncertainty associated with these different climate model projections (Burke et al., 2015).

Figure 3: *Future intensity of droughts (as deviations from the reference period of 1979–2020) for the near (2020–2049) and more distant (2030–2059) future, under the RCP 8.5 scenario and by GCM*

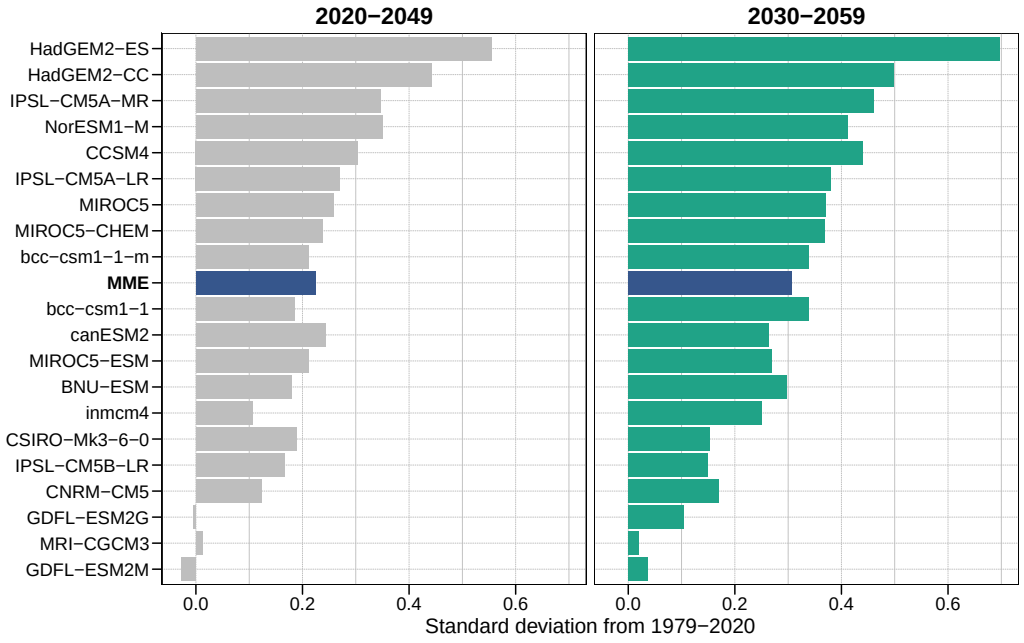

Note: The plots on the left (right) side show the distribution of future drought severity (as deviations from the reference period of 1979–2020) for the near (more distant) future across 20 downscaled GCMs and the multi–model ensemble average. See Table D.1 in Appendix D for a detailed overview of the results.

3. Empirical framework

3.1. The sample

We construct a county-level panel dataset from Agricultural Censuses maintained by the National Agricultural Statistics Service (NASS) of the USDA and for the following census years: 2002, 2007, 2012, and 2017.[14] A county–level analysis is more appropriate to evaluate the potential benefits of agricultural policy, since analyzing government payments at the individual farm level may reflect individual strategic choices and characteristics of the farm operation (Goodwin et al., 2011). Additionally, it allows us to exploit the diversity of agricultural production patterns, the large cross–county variation in observed and future weather patterns and the sensibility of agricultural production to local climate across the CONUS.

US farm programs are updated about every 5 years through a comprehensive package of legislation known as the Farm Bill. An important consideration when analyzing these programs is that the amount of support they provide may vary greatly from year to year, as agricultural programs are highly dependent on the market and weather conditions of each year (Goodwin et al., 2011). Our analysis relies upon several census years of data (2002, 2007, 2012, and 2017 agricultural censuses), which makes it easier to generalize our results. Additionally, there has been a significant change in agricultural policy since the Farm and Agricultural Improvement and Reform (FAIR) Act of 1996, which has shifted policy away from government involvement and toward more market–oriented policies. By using data from the 2002 to 2017 census years, we are able to analyze federal farm programs, which cover three Farm bills (2002, 2008, and 2014) and broadly share the same design.

We first extract government payment data from each census year, including loan deficiency payments, disaster payments, and all annual direct payments and counter-cyclical payments as defined under the the 2002 and 2008 Farm bills, and those specified in the 2014 Agricultural Act (Agriculture Risk Coverage and Price Loss Coverage). This definition only covers income support programs, that are designed to stabilize farmers' earnings through three specific program mechanisms: direct payments, market loss assistance and counter–cyclical payments, and loan deficiency payments and marketing loans (Goodwin et al., 2011). We, therefore, exclude programs from the Federal Crop Insurance Program that provide subsidized insurance to mitigate risk in agriculture (Crane-Droesch et al., 2019) and annual rental revenues from conservation programs designed to prompt changes in land use or production practices (Claassen et al., 2007).[15]

We construct a measure of net returns from the market at a county level by taking the average

[14] The Census is conducted every five years and is administered to all farms and ranches (in rural or urban settings), producing and potentially selling at least $US 1,000 of their products. The Census is the only source of detailed county–level agricultural data collected, tabulated, and published using a uniform set of definitions and methodology.

[15] We also exclude Commodity Credit Corporation proceeds, and payments from state and local government agricultural programs.

difference between total agricultural sales receipts (excluding government payments) and total production costs (including all expenses, marketing charges, hauling fees, other fees, and income taxes), following Goodwin et al. (2011).

We calculate all sources of income at the county level and per operation.[16] This is done by dividing the total net returns from the market and income support payments from federal farm programs in a specific county by the total number of operations in that county. To account for price changes and ensure accurate comparisons over time, net returns from the market and income support payments are deflated to 2011 constant dollars using the index of agricultural prices.

Table 1 reports county–level summary statistics for the census years 2002, 2007, 2012, and 2017. After considering all missing observations due to disclosure controls and removing singleton observations, we obtain an unbalanced panel of 9607 counties, which represents an average time dimension of 3.56 years for 2696 counties.

Table 1: *Summary descriptive statistics, CONUS*

	2002	2007	2012	2017
Sample				
Number of agricultural counties	2,417	2,452	2,404	2,334
Number of operations	1,861,812	1,940,867	1,833,158	1,706,287
Mean number of op. by county	770.30	791.54	762.54	731.06
Income support payments ($US 2011 prices)				
Mean payments	3,348,811	2,785,817	2,364,118	2,995,012
Median payments	2,098,418	1,570,312	1,558,040	1,715,591
Mean payment per operation	4,347.41	3,519.49	3,100.31	4,096.81
Net returns from the market ($US 2011 prices)				
Mean net returns	14,017,688	21,842,136	20,985,012	21,075,026
Median net returns	3,151,142	8,774,639	8,076,118	8,456,452
Mean net returns per operation	18,197.70	27,594.48	27,519.88	28,828.04

Note: Income support payments and net returns from the market are adjusted for agricultural prices fluctuations using the agricultural price index with base year 2011. An agricultural county corresponds to a county with more than 10,000 acres $\approx$ 40 km2 agricultural land (cropland or pasture/hay).

From 2002 to 2017, the number of farm operations per county varied between 731 and 790, with a downward trend since 2007. The average net returns per operation increased from $US 18,197 to $US 28,828. The average income support payments per operation was more variable, reaching $US 4,347, $US 3,519, $US 3,100, and $US 4,097 in 2002, 2007, 2012, and 2017, respectively.

[16] Defining net returns and government payments per operation helps to ensure that the measurement is not affected by the differences in county sizes across the United States.

Table 2 presents statistics on the frequency of drought events, classified by severity, among the various climate regions of the United States from 2002 to 2017.

Table 2: *Relative frequency of wetness/dryness events over the CONUS distributed by Köppen-Geiger climate classes, census years (from 2002 to 2017)*

		% of total CONUS counties						
	Weather conditions	Köppen–Geiger			Census years			
		B	C	D	2002	2007	2012	2017
$Dry \geq 1$	Dry	23.85	19.86	21.34	5.41	27.78	49.35	0.16
$0.5 \leq Dry < 1$	Slightly dry	23.19	17.55	18.00	17.43	23.61	27.62	4.82
$-0.5 \leq Dry < 0.5$	Near normal	41.80	49.42	49.36	66.43	36.57	20.19	71.27
$-1 \leq Dry < -0.5$	Slightly wet	8.19	11.20	8.78	9.22	8.53	2.21	20.81
$Dry \leq -1$	Wet	2.62	1.56	2.45	1.30	3.84	0.10	2.54

Note: Positive (negative) values of Dry indicates drier (wetter) conditions. Frequencies by hydro–climatic conditions are calculated at the county level over the CONUS for each census year. Dominant regional climate zones B, C and D are defined according to the Köppen–Geiger climate classification (see Peel et al. (2007) for a description of the classification). Zone B: arid or dry zone, Zone C: warm/mild temperate zone, Zone D: continental zone.

The severity of drought episodes has fluctuated throughout the studied period. In 2012, the United States experienced its most intense drought since the 1950s (Rippey, 2015), with approximately 50% of its land area affected. In contrast, 2002 and 2017 saw much milder conditions, with less than 23% and 6% of US counties in drought, respectively. Overall, normal weather conditions prevailed on average and drought events were evenly distributed across all climate zones. This provides evidence that our study will not be affected by sample–selection bias.

3.2. Identification and empirical strategy

The primary goal of our analysis is to assess by how much income support payments from federal farm programs increase in a county when the net returns of this county decrease due to drier–than–normal conditions. For a county c, the net cash farm income ($CASH_c$) corresponds to the sum of the net returns from the sale of agricultural commodities (INC_c) and the income support payments from federal farm programs (GOV_c):

$$\Delta CASH_c = \Delta INC_c + \Delta GOV_c \tag{2}$$

Let income support payments be a function of net returns, so that every 1 percent decrease in net returns results in a β percent increase in income support payments. That is,

$$\beta = -\frac{\Delta GOV_c / GOV_c}{\Delta INC_c / INC_c} \tag{3}$$

$$\Delta CASH_c = \lambda \Delta INC_c \text{ with } \lambda = 1 - \beta \times \frac{GOV_c}{INC_c} \tag{4}$$

Equation 4 illustrates the income–stabilization capacity of income support payments. It tells us that, if a county experiences a negative one-dollar shock to its net returns, its net cash farm income will decrease by less than one dollar ($1 - \beta \times GOV_c/INC_c$ cents). Our empirical strategy is then to estimate the elasticity β using county-level data with the following empirical specification:

$$GOV_{c,t} = \alpha + \beta INC_{c,t} + \epsilon_{c,t} \tag{5}$$

where $GOV_{c,t}$ and $INC_{c,t}$ refer to income support payments and net returns per operation of a county c at a given date t, respectively.

To ensure that we are not picking up effects at the US level, we consider county-level income support payments and net returns relative to their CONUS level ($GOV_{US,t}$ and $INC_{US,t}$). Identification comes, therefore, only from within-county variations, eliminating any concerns of time-trending unobservables at the federal level.[17] The modified equation is therefore the following:

$$Gov_{c,t} = \alpha + \beta Inc_{c,t} + \epsilon_{c,t} \tag{6}$$

where $Gov_{c,t} = GOV_{c,t}/GOV_{US,t}$ and $Inc_{c,t} = INC_{c,t}/INC_{US,t}$.

Since the relevant variables are now expressed in relative terms, the coefficient β measures the percentage change in a county's income support payments (relative to the rest of the CONUS) when its net returns from the market change by 1%, holding constant the changes in CONUS aggregate net returns. The magnitude of β represents, therefore, the average size of the income–stabilization effect provided by income support payments.

Because our main goal is to assess the capacity of income support payments to offset income losses caused by drought conditions, we employ an instrumental variables (IV) approach and use our drought index time series, as defined in equation 1, as excluded instruments for net returns. This approach allows us to focus on income support payments that are specifically meant to offset losses caused by drought events. Moreover, it addresses endogeneity concerns inherent to policy variables. Payments from federal farm programs can shape farm income, making reverse causality a likely

[17] Moreover, reasoning in relative terms enables us to deal with counties characterized by a negative net return (33.1% of all observations). The conventional technique of replacing negative values by missing values with for negative values cannot be employed in our study. Negative values are taken into account when calculating net returns and therefore impact federal payments. Consequently, using the log transformation is not feasible. Adding a constant value to the data would also be inappropriate, by creating a problem of adequacy with what would happen with government payments. Finally, reasoning in relative terms allows us to mitigate the differences between counties due to price differences and to consider the distribution of the total budget among agricultural producers.

feature of our specification (Westcott and Young, 2004; Weber and Key, 2012).[18] For instance, areas that receive more payments can experience an increase in crop yields and higher subsequent net returns from the market. Such endogeneity concerns motivate an IV approach to estimate the income–stabilizing capacity of income support payments more reliably.

However, instrumenting net returns using an index of drought severity raises two issues. First, the choice of net returns as a proxy of farm incomes implies omitting storage activities that farmers may employ to smooth out the impact of drought on their income over time. Fisher et al. (2012) points out that this may lead to an endogeneity bias toward zero. While this argument is persuasive, a careful examination of storage activities would require an extended panel dataset with more comprehensive information on farmer behavior that the census data do not provide. Additionally, including temporal fixed effects may partially address this issue. The other concern is that droughts can affect other outcomes that may also influence income support payments. Because of this, two–stage least squares (2SLS) estimates based on our instruments can be biased as the assumption that droughts only affect payments from federal farm programs through their effect on net returns may be no more valid. To address this issue, we include relevant control variables, $X_{c,t}$, in our specification to make the exclusion restriction assumption plausible. First, we control for the proportion of agricultural irrigated land. Indeed, omitting the irrigation process usually results in an important bias, leading to less damaging projected climate impact estimates for US agriculture, as irrigated yields tend to be higher and less variable than rainfed yields (Schlenker et al., 2005). We also control for the importance of cropland areas as a percentage of total agricultural land. Federal farm programs target certain field crops (e.g., corn, soybeans, and wheat) and may therefore provide higher payments to areas where these crops are grown. Finally, we account for the concentration of agricultural production at the county level. Drought episodes can impact the concentration of agricultural production, since risk mitigation measures, such as diversifying production across crops, may be less effective on smaller farms (Ramcharan, 2010). As a result, droughts, by altering the distribution of farm sizes, can influence income support payments.[19]

We therefore estimate a two-stage model of the following form:

$$Inc_{c,t} = a_c + B'Dry_{c,t} + \omega' X_{c,t} + \phi \text{year}_t + e_{c,t} \tag{7}$$

and

$$Gov_{c,t} = a_c + \beta \widehat{Inc}_{c,t} + \Gamma' X_{c,t} + \gamma year_t + \upsilon_{c,t} \tag{8}$$

[18] Even decoupled payments may have some allocative ("coupling") effects due to uncertainty, imperfect credit, labor and land markets, and farmer expectations for future payments (see Bhaskar and Beghin (2009) for detailed mechanisms).

[19] Table C.1 in Appendix C presents the summary descriptive statistics of the control variables.

where counties are indexed by c and years are indexed by t. $Inc_{c,t}$ is county's c net returns from the market relative to the total amount at the CONUS level (in % of total \$US per 1000 operations); $Gov_{c,t}$ is county's c income support payments relative to the total amount at the CONUS level (in % of total \$US per 1000 operations); $X_{c,t}$ is the vector of included instruments. a_c captures time–invariant county factors and $year_t$ captures the aggregate time effect in period t that is common among all counties.

Identification in this two–stage model arises from drought measures, indicated by the vector $Dry_{c,t}$ in equation 7, calculated as contemporary values of monthly negative SPEI aggregated over the crop–growing season (as in equation 1) and used as instrumental variables for net returns from the market. The parameter B' measures net returns' sensitivity to drought and is expected to be negative.[20] In equation 8, the parameter of interest is β, which measures the capacity of income support payments to mitigate net return losses caused by drier conditions. β is expected to be negative if these payments are effective.

4. Results

4.1. Results for the CONUS

Table 3 presents our results for the CONUS. The first-stage conditional correlations suggest that drier–than–normal conditions negatively impact net returns per operation. The base specification in column 1 shows that the drought index (Dry) is negative and significant. The evidence also suggests that lower net returns are significantly associated with higher income support payments. The IV baseline estimate in column 2 implies that a 1% decrease in a county's net returns relative to the CONUS leads to an increase of 0.36% in income support payments. The results of the hypothesis tests at the bottom of Table 3 show that our instrument meets the exclusion assumptions and provides reliable and unbiased estimates, by successfully addressing the issue of endogeneity.[21] The estimated coefficients for the control variables (columns 3 and 4) are in close agreement with existing literature, suggesting that net returns from the market are positively correlated with land concentration, irrigation, and cropland areas. Additionally, land concentration and cropland areas also positively affect income support payments (Schlenker et al., 2005; Ramcharan, 2010). Our findings are little changed when the control variables are added to the model, supporting our assumption that drought effects on income support payments work primarily through changes in net returns.

[20] Following Burke and Emerick (2016), we choose to specify a linear impact of weather. These authors build on the argument of McIntosh and Schlenker (2006) that including a quadratic term in the standard panel fixed effects model allows unit means to re-enter the estimation and can therefore raise omitted variables concerns.

[21] The Kleibergen–Paap rk Wald F statistic suggests that our instrument is strong enough to predict net returns from the market. The Kleibergen–Paap LM statistic is also significant and rejects the null hypothesis of under–identification.

Table 3: *Benchmark results, CONUS average, 2002-2017*

	Without control variables		With control variables	
	1st stage	2nd stage	1st stage	2nd stage
	(1)	(2)	(3)	(4)
Dry	-0.0069***		-0.0071***	
	(0.0014)		(0.0013)	
Inc		-0.3621***		-0.3569***
		(0.1325)		(0.1260)
Irrigation			0.0038***	0.0014*
			(0.0009)	(0.0008)
Field crop			0.0317***	0.0280***
			(0.0089)	(0.0059)
Concentration			0.0145**	0.0358***
			(0.0060)	(0.0048)
N		9607		9607
F-stat		7.4728		17.886
KP F-stat		26.194		27.827
KP-LM test		25.794***		27.390***

Note: The excluded instrument is the drought index (equation 1). A rise in this index reflects drier conditions. *, **, and *** indicate significance at the 10%, 5% and 1% levels, respectively. The first-stage F-statistic is used to investigate the strength of the instruments. The Kleibergen and Paap Wald rk F statistic tests if the excluded instruments are weak (weak identification). The null hypothesis of the Kleibergen–Paap rk LM statistic, KP LM-stat, is that the equation is under–identified. Robust standard errors clustered by Federal Information Processing System (FIPS) codes are reported in parenthesis.

We conduct a robustness analysis to evaluate the stability and reliability of our estimated coefficients. First, we account for a potential persistent effect of droughts by including a temporal effect of our drought index. The results show that the first lag of our drought index is insignificant, while the variable's coefficient remains negative and significant contemporaneously, suggesting that contemporaneous drier–than–normal conditions explain most of the observed variability in net returns per operation. Lower net returns are still significantly associated with higher income support payments, indicating that these payments absorb 32% of income losses due to an adverse drought episode (see Table C.2 in Appendix C). We also perform a placebo test, dividing counties into metropolitan and non-metropolitan based on Rural–Urban Continuum Codes (2013).[22] As expected, our findings

[22] https://www.ers.usda.gov/data-products/rural-urban-continuum-codes.aspx. The Rural–Urban Continuum Codes (RUCC) is a classification system developed by the USDA to categorize US counties into different levels of rurality or urbanization. The codes are based on a county's population size, degree of urbanization, and proximity to larger urban areas. The system assigns each county a code ranging from 1 to 9, with 1 representing the most urban counties and 9 representing the most rural counties. We consider counties as metropolitan if they belong

indicate that the sensitivity of net returns to drought events and the income-stabilizing effect of income support payments are insignificant in metropolitan areas where farming is relatively unimportant. In contrast, the results for non-metropolitan areas are comparable to the CONUS average (see Table C.2 in Appendix C). Finally, we test the sensitivity of our estimates using an alternative drought index, the Palmer Drought Severity Index (PDSI) developed by Palmer (1965).[23] The results from this index largely corroborate those from our benchmark index (see Table C.3 in Appendix C).

4.2. Heterogeneity across the CONUS

Our robustness analysis confirms that droughts have a significant impact on net returns, and income support payments play an important role in mitigating 36% of the associated income losses at the CONUS level. However, these results do not take into consideration the effects of more localized climate conditions, which can be masked at the CONUS level, due to the diversity of crops produced (Kuwayama et al., 2019). To accurately capture the heterogeneous impact of drought conditions, we extend our analysis to include several major commodity crops that account for 90% of total US crop production.

We utilize the proportional scores of county acreage values for 22 key crops from Hammond Wagner et al. (2019). For each county, we sum up these scores to define three agricultural crop production categories based on seven main commodity crops: (i) corn and soybeans, (ii) hay (alfalfa and grasses), and (iii) wheat, barley, and cotton. By doing so, we identify the geographic specialization in the production of these major commodity crops at the county level across the CONUS, considering the share of each county in the production of each major crop category. This approach is more advantageous than relying on regional divisions, as the definition of agricultural regions can be problematic. Some counties may contribute significantly to the production of a crop type without belonging to a dominant region, and there is often disagreement about how to define agricultural regions (like the Corn Belt). By considering county-level crop acreage shares, we minimize the potential for such biases related to regional classifications and can better apprehend the range of crops produced and agricultural practices (e.g., crop rotation) at a local level.

Figure 4 shows the resulting geographic specialization in crop categories across US counties. Our categorization reflects the main agricultural areas of specialization in the United States, with corn and soybeans primarily grown in the Midwest, and wheat and barley mainly cultivated in the Great Plains and Columbia River Basin. In contrast, hay production is more widely distributed throughout the United States, with significant production in various western and southeastern

to the first two categories, i.e., in case of metropolitan areas with a population of more than 250,000.

[23] We use the PDSI as it is widely used and the climate variables necessary for its calculation are available in the gridMET dataset.

states. We further confirm the accuracy of our categorization through a Spearman's correlation analysis between the weights of the different crops, with significant results at the 95% probability level.[24]

Figure 4: *Typology of agricultural crop production in the United States and importance of main major commodities acres by county, 2012*

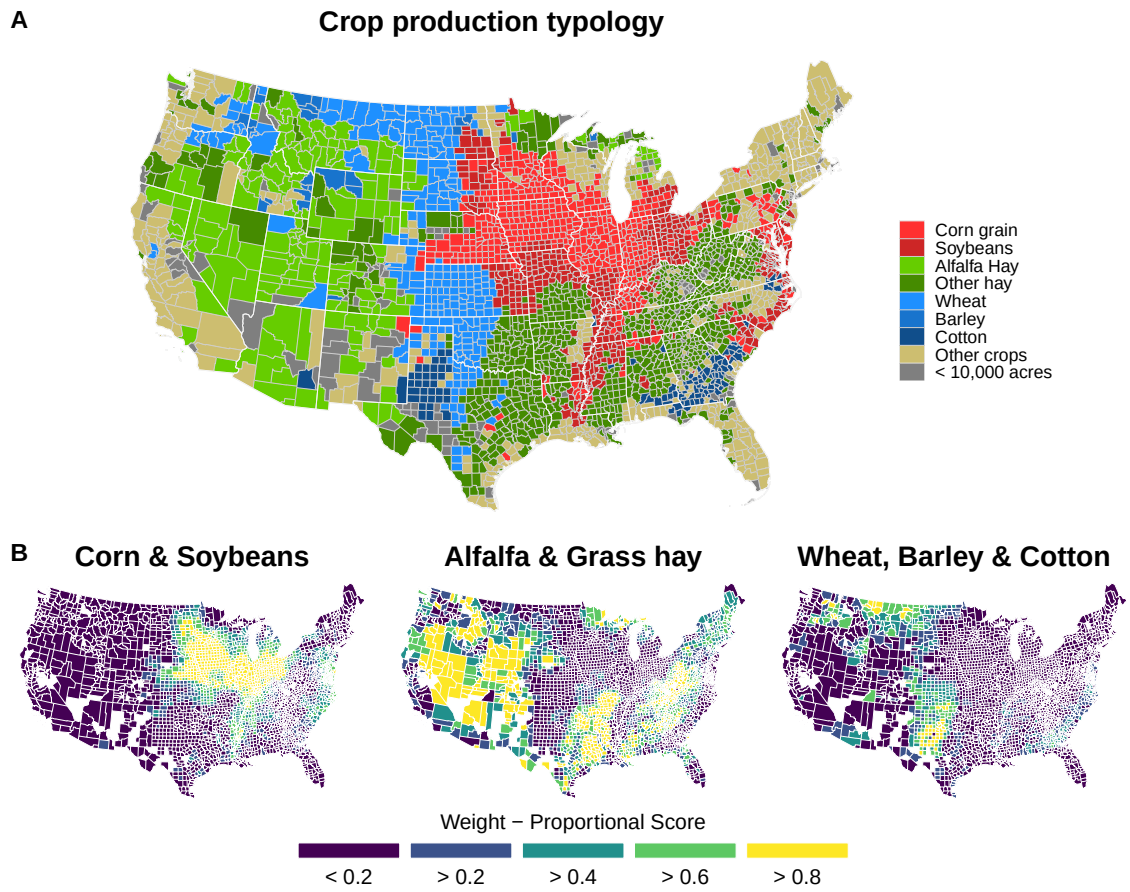

Note: Map A shows the distribution of crop acreage across the United States, as calculated by Hammond Wagner et al. (2019). Map B shows the spatial distribution of main commodity crop-specific shares, which are calculated by adding up the proportional acreage scores of each major crop in each crop category.

The proportions of major crop commodities produced by each county are then used as probability

[24] We use the Spearman's correlation instead of the Pearson's linear correlation because our data is not normally distributed. The results of the pairwise correlations are shown in Table C.4 in Appendix C. We find one inverse association between barley and cotton among all crops that belong to the same category. We repeat our estimations without including cotton in our categorization. The results, which are available upon request from the authors, remain unchanged.

weights to estimate the model in equations 7 and 8. Table 4 reports the results of the weighted 2SLS estimates. They show the varying degree of drought sensitivity among crops, with wheat, barley and cotton exhibiting the highest sensitivity. They also provide evidence of the capacity of income support payments to smooth net returns losses due to drought episodes for all major commodity crops, highlighting the importance of support for key crop producers in US farm policy. Specifically, the coefficient β is always significant and negative, with values ranging from -0.28 to -0.35 among the three crop categories.

Table 4: *Results for major commodity crops, weighted 2SLS, 2002-2017*

	Corn & Soybean		Alfalfa & Grass hay		Wheat, Barley & Cotton	
	1st stage	2nd stage	1st stage	2nd stage	1st stage	2nd stage
	(1)	(2)	(3)	(4)	(5)	(6)
Dry	-0.0096***		-0.0062***		-0.0144***	
	(0.0012)		(0.0010)		(0.0025)	
Inc		-0.3473***		-0.3451***		-0.2766**
		(0.0876)		(0.0842)		(0.1169)
Irrigation	0.0024**	0.0006	0.0024***	0.0014***	0.0038**	0.0004
	(0.0011)	(0.0007)	(0.0009)	(0.0005)	(0.0019)	(0.0012)
Field crop	0.0206**	0.0287***	0.0254***	0.0202***	0.0233**	0.0285***
	(0.0093)	(0.0060)	(0.0088)	(0.0041)	(0.0117)	(0.0085)
Concentration	0.0100	0.0361***	0.0202**	0.0192***	0.0209**	0.0513***
	(0.0070)	(0.0057)	(0.0067)	(0.0038)	(0.0095)	(0.0082)
N		8687		9377		8750
F–stat		15.782		17.59		13.230
KP F–stat		58.311		43.569		32.872
KP–LM test		53.415***		42.374***		31.803***

Note: The excluded instrument is the drought index (equation 1). A rise in this index reflects drier conditions. *, **, and *** indicate significance at the 10%, 5% and 1% levels, respectively. The first-stage F-statistic is used to investigate the strength of the instruments. The Kleibergen and Paap Wald rk F statistic tests if the excluded instruments are weak (weak identification). The null hypothesis of the Kleibergen–Paap rk LM statistic, KP LM–stat, is that the equation is underidentified. Robust standard errors clustered by Federal Information Processing System (FIPS) codes are reported in parenthesis.

From these estimates, we deduce the average loss in net returns in $US per operation due to a one-standard deviation increase in the drought index and the subsequent average increase in income support payments in $US per operation.[25] Figure 5 shows these predicted economic outcomes, for both the entire CONUS (for any crop category) and individual crop categories. To accurately represent crop production across the entire CONUS, the outcomes for each crop category are calculated by averaging predictions for counties located in areas where the crop category is dominant, as depicted by map A in Figure 4 (turquoise bars), and by their relative share in total cultivated areas across the entire CONUS (green bars).

The amount of income support payments per operation in response of drought conditions varies among crop categories. This variation comes from two sources: the sensitivity of crops to drought conditions and the income-stabilizing capacity of income support payments. For instance, alfalfa and grass hay, which are less sensitive to drought conditions, exhibit the lowest income support payment per operation of $US 32.1 (2011 prices). In contrast, corn and soybean have the highest level of income support payments per operation ($US 70.7 2011 prices) due to a greater capacity of these payments to mitigate net returns' losses caused by drought. Due to an acreage-size effect, predicted income losses and income support payments for the CONUS are clearly tied to corn and soybean-producing areas, which account for about 50% of the total outcomes. Lastly, crop areas that are more sensitive to drought conditions do not necessarily have a higher capacity for income stabilization through income support payments. Instead, the degree of income–stabilization is more closely related to the percentage of cultivated areas across the entire CONUS, mirroring the current design of the US agricultural policy, with payments from federal farm programs mainly based on acres historically planted to program crops ("base acres") and cropping patterns.

[25] The coefficient β measures the effect of a 1% drop in a county's net returns, caused by drier–than–normal conditions on income support payments that the county receives in comparison to the CONUS. When average cash incomes decrease by one–dollar, average income support payments increase by $\widehat{\beta} \times {}^{Gov}/_{\widehat{Inc}}$.

Figure 5: *Predicted losses in net returns and increases in income support payments due to drought conditions for the CONUS and crop categories, average over the 2002–2017 period*

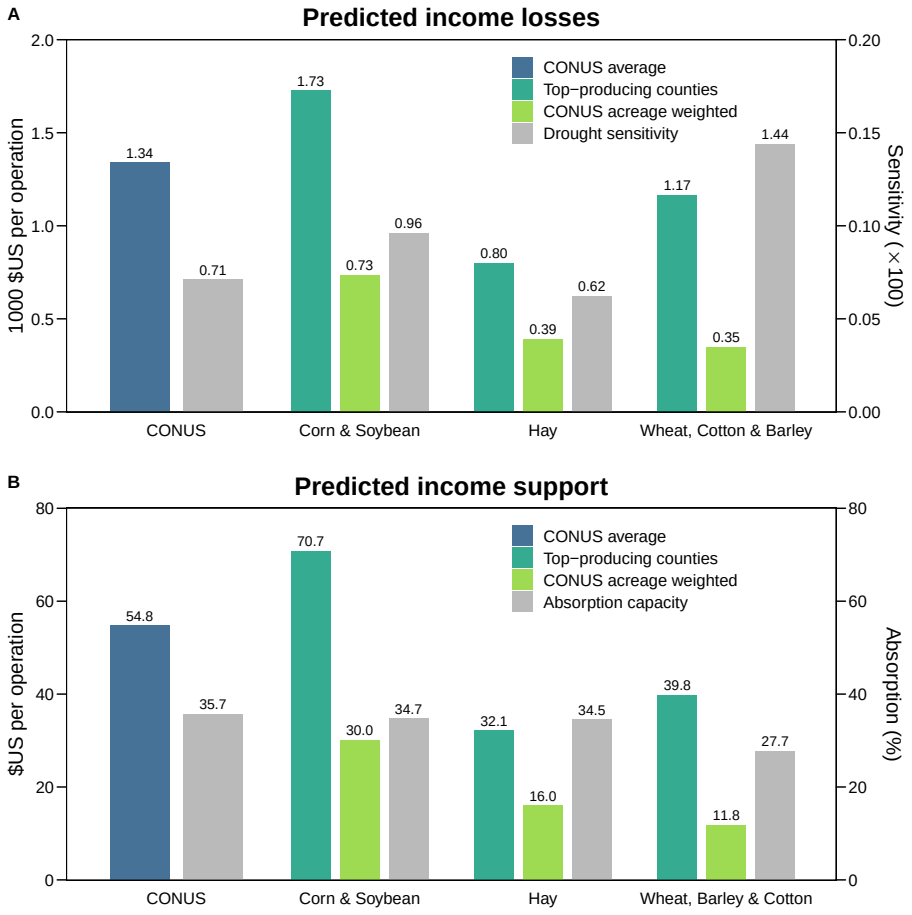

Note: The bar graphs show average predicted losses in net returns and increases in net income support payments due to drought conditions for the CONUS level and crop categories from 2002–2017. The turquoise bars indicate the average predictions for dominant production areas. The green bars show the average predictions weighted by acreage for all cultivated areas across the entire CONUS. The gray bars denote the size of net returns' sensitivity to drought events (× 100) and the percentage of income stabilization provided by income support payments for the CONUS and crop categories derived from our estimate results.

4.3. Regression uncertainty

Our estimated parameters based on historical data provide insights into the relationship between net returns and income support payments under existing climate conditions. They also serve as benchmarks for evaluating the expected costs of mitigating farm income losses due to drier conditions under climate change. As such, it is essential to fully grasp the uncertainties surrounding these

parameters due to their implications on policy recommendations. Indeed, without a reliable assessment of the uncertainty surrounding average estimates, the costs of stabilizing farm incomes may be inconsistent. In addition, estimating these uncertainties can play an essential role in identifying potential risks and formulating contingency plans, ultimately fostering more effective decision-making in agricultural management.

The traditional way to estimate the uncertainty of regression coefficients is to use parametric standard errors, which are based on the assumption that errors follow a normal distribution. However, this assumption may not always be valid, leading to incorrect assessments of the standard errors. To ascertain the statistical uncertainty of our mean estimates, we estimate block bootstrap regression coefficients from our main specifications, for both the CONUS and crop categories. We generate a distribution of estimated parameters and their corresponding confidence intervals based on 10,000 repetitions by repeatedly resampling the data (with replacement) and clustering the resampled data into groups at the county level.

The results from the bootstrap regression analysis are reported in Table 5.[26] They show low mean bias, indicating that our model accurately estimates the coefficients for net returns' sensitivity to drought (Dry) and the income–stabilization capacity of income support payments (Inc). Sensitivities of net returns to drought are notably robust, as demonstrated by the close alignment between bias–corrected and accelerated confidence intervals (BCa) derived from bootstrapped estimates and the analytical confidence intervals. However, the bootstrapped confidence intervals for income–stabilization capacities of income support payments exhibit a noticeable downward shift. This shift toward more negative values suggests that the distribution of these coefficients deviates from what was initially expected using the traditional parametric approach. Consequently, this affects the level of confidence associated with these coefficients and ultimately the predicted values of income support payments.

Figure 6 shows the distribution of bootstrapped estimated income support payments by operation and 95% BCa empirical confidence intervals for the CONUS and crop categories. For comparison, the graphs also show the distributions that are implied by the estimated coefficients and their standard errors (assuming normality) from our parametric estimations. The uncertainty in income-stabilization coefficients from block bootstrap estimates results in a wider range of plausible values for income support payments mainly located in the upper part of the distribution. Indeed, while the average predicted values estimated from the resampled data and parametric estimates are close, their distributions exhibit different shapes. The bootstrapped estimates are slightly more skewed to the right, indicating a higher probability of observing larger-than-average predicted values of income support payments.

[26] The complete results from the block bootstrap regressions are available upon request.

Table 5: *Non–parametric bootstrapped estimates at the CONUS level and by crop categories, 2002–2017*

		CONUS level		Crop categories					
				Corn & Soybean		Alfalfa & Grass hay		Wheat, Barley & Cotton	
		Dry	Inc	Dry	Inc	Dry	Inc	Dry	Inc
Coefficients									
Mean estimate		-0.00747	-0.3488	-0.0096	-0.3473	-0.0064	-0.3472	-0.0147	-0.2799
Median estimate		-0.00750	-0.3368	-0.0098	-0.3386	-0.0064	-0.3373	-0.0147	-0.2695
Bias		-3.952e-04	8.009e-03	-1.527e-4	1.642e-3	-1.463e-04	-2.078e-03	-3.183e-4	-3.296e-3
Standard errors									
Bootstrapped		0.00139	0.1200	0.0014	0.0961	0.00103	0.0864	0.00248	0.1069
Asymptotic		0.00134	0.1260	0.0012	0.0876	0.00095	0.0842	0.00250	0.1169
Confidence Intervals (95%)									
Analytical	Lower	-0.0097	-0.6039	-0.0123	-0.5374	-0.0081	-0.5101	-0.0192	-0.5057
	Upper	-0.0044	-0.1098	-0.0067	-0.1605	-0.0044	-0.1800	-0.0094	-0.0475
Percentile	Lower	-0.0102	-0.6201	-0.0125	-0.5533	-0.0084	-0.5467	-0.0194	-0.5236
	Upper	-0.0048	-0.1495	-0.0070	-0.1745	-0.0044	-0.2063	-0.0098	-0.0982
BCa	Lower	-0.0094	-0.6884	-0.0122	-0.5806	-0.0081	-0.5729	-0.0187	-0.5451
	Upper	-0.0039	-0.1788	-0.0067	-0.1899	-0.0041	-0.2192	-0.009	-0.109

Note: Mean and median estimated coefficients are retrieved from the coefficient distributions obtain from 10,000 replications. Asymptotic Standard errors and 95% analytical confidence intervals are shown for the sake of comparison. 95% confidence intervals calculated from block bootstrap regression are obtain using the percentile method and the Bias Corrected and accelerated method (BCa).

Figure 6: *Statistical uncertainty surrounding estimated income support payments, average over the 2002–2017 period*

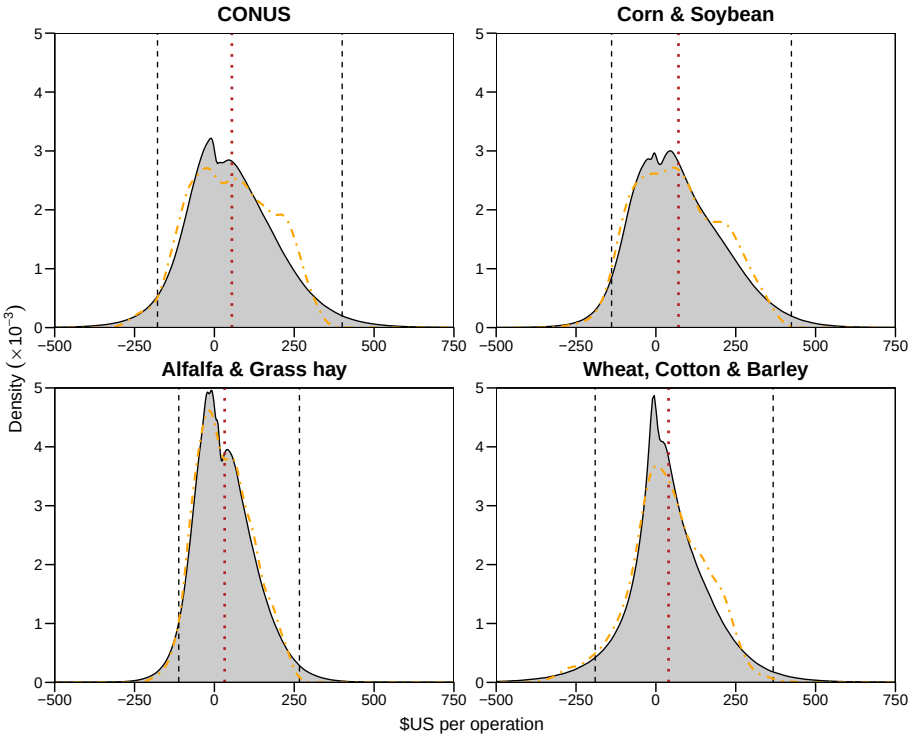

Note: The black dotted lines represent the BCa 95% confidence intervals (CI) calculated. The mean predictions (red dotted lines) as well as the entire distribution of predicted income support payments obtained at the county level from block bootstrapped estimates (with 10,000 repetitions) are calculated from counties producing predominantly at least one of the crops belonging to the category. The orange curve represents the predicted income support distribution estimated from the parametric model. The predicted mean income support payments and the associated confidence intervals are the following: CONUS $US 54.8 per operation [95% CI: -178.083 ; 400.121]; corn and soybean: $US 70.7 per operation [95% CI: -138.745 ; 424.282]; alfalfa and grass hay: $US 32.1 per operation, [95% CI: -111.502 ; 266.286] ; wheat, barley, and cotton: $US 39.8 per operation [95% CI: -190.014 ; 367.150].

Overall, our findings suggest that our mean estimates can be used as unbiased benchmarks for assessing the potential impacts of climate change. Moreover, using non-parametric bootstrapped estimates provides a more accurate assessment of the possible extreme values in the cost of smoothing income losses caused by drought events. A more accurate apprehension of these costs for the whole CONUS and major commodity crops is especially relevant in predicting their future trends under climate change, as the effects of climate change are also uncertain and can have far-reaching impacts.

5. The cost of stabilizing farm incomes under climate change

Our final empirical exercise aims to quantify how much additional income support payments would be needed to maintain their income stabilization capacity under global warming. Accordingly, we compare the cost of stabilizing farm incomes when counties are subject to their observed 2002–2017 climate, with the cost that would be observed if they experience future climate conditions from 2020–2049 and 2030–2059 under the RCP 8.5 scenario.

5.1. Empirical Implementation

We first develop "counterfactual" drought index time series wherein drought events will occur in the future by using projected drought index data for each county over the periods 2020–2049 and 2030–2059. Formally, $Dry_{c,t}$ represents the drought index value in a county c at time t during the studied period (2002-2017), and $\Delta Dry_{c,h}$ is the future average change in hydro–climatic conditions based on the RCP 8.5 scenario, where h is the forecast horizon.

Denoting the counterfactual drought conditions for any county c as $Dry_{c,t}+\Delta Dry_{c,h}$, we can deduce the associated change in net returns from the market due to climate change:[27]

$$\Delta\widehat{Inc}_{c,t} = \widehat{B'}\left(Dry_{c,t} + \Delta Dry_{c,h}\right) - \widehat{B'}Dry_{c,t} \tag{9}$$

The counterfactual level of income support payments that would be needed to offset the impact of future drought conditions on net returns can thus be derived as follows:

$$Gov_{c,t} + \Delta Gov_{c,h} = \widehat{\beta}\left(\widehat{B'}Dry_{c,t} + \Delta\widehat{Inc}_{c,h}\right) \tag{10}$$

Most studies that assess the economic impacts of climate change use mean regression coefficients from parametric regression models and an average from multiple climate models to project impacts of predicted climate change. Instead of relying on these two common simplifications, we follow the recommendation of Burke et al. (2015) and account for both the uncertainty in the regression coefficients (statistical uncertainty) and the uncertainty in the climate models (climate uncertainty) when projecting future income support payments.

To do so, we consider the non-parametric bootstrapped coefficients of our main specification and climate projections from the CMIP5 20 downscaled GCMs to estimate a range of possible future drought conditions and income support payments levels under the RCP 8.5 scenario. We then compare three sets of projections to determine the impact of uncertainties in both the regression coefficients and the climate models on projected income support payments for the CONUS and each

[27] Projected counties net returns and income support payments levels are treated as nuisance parameters and are absorbed by multiple fixed effects and controls in equations 7 and 8.

crop category. Our first set of projections (a) relies on fixed changes in climate conditions projected with the MME average, while the regression coefficients for both the sensitivity of net returns to drought and the income–stabilization capacity of income support payments are allowed to vary. Our second set of projections (b) accounts for uncertainty in the climate models by allowing the climate projections to vary between the minimum and maximum drought projected values, while keeping the regression coefficients at their point estimates. In our third set of projections (c), we consider regression coefficients and climate model uncertainties, by allowing both climate projections and regression coefficients to vary.

5.2. Projections of income support payments

Figure 7 shows the projected income support payments for the CONUS and crop categories for the near (2020–2049) and more distant (2030–2059) future according to our first set of projections. The graphs also include the predicted levels of income support during the studied period (2002–2017) for comparison.

The values shift markedly to the right over time, indicating a shift in income support payments to larger amounts per operation. Precisely, under the RCP 8.5 emissions scenario, income support payments at the CONUS level are forecasted to reach an average of $US 99 and $US 116 (2011 prices) per operation with drought conditions projected over 2020–2049 and 2030–2059, compared to $US 55 (2011 prices) per operation over the studied period (2002–2017). Our mean estimates imply that income support payments per operation would be about 111% higher relative to the 2002–2017 period if future climate conditions over 2030-2059 prevailed. Wheat, barley, and cotton are expected to see the most significant growth in income support payments over both forecast periods, with increases of 115% for 2020–2049 and 156% for 2030–2059. Alfalfa and grass hay are also expected to see significant growth, with increases of 97% for 2020–2049 and 129% for 2030–2059. Despite a relatively lower projected growth rate in income support payments (+55% for 2020–2049 and +75% for 2030–2059), corn and soybean are expected to remain the most subsidized crops under climate change. Although their contribution to the total cost is projected to decrease, they should still account for more than 46% of future income support payments.

Figure 7: *Projected income support payments at the CONUS level and by crop categories, multi-model ensemble average*

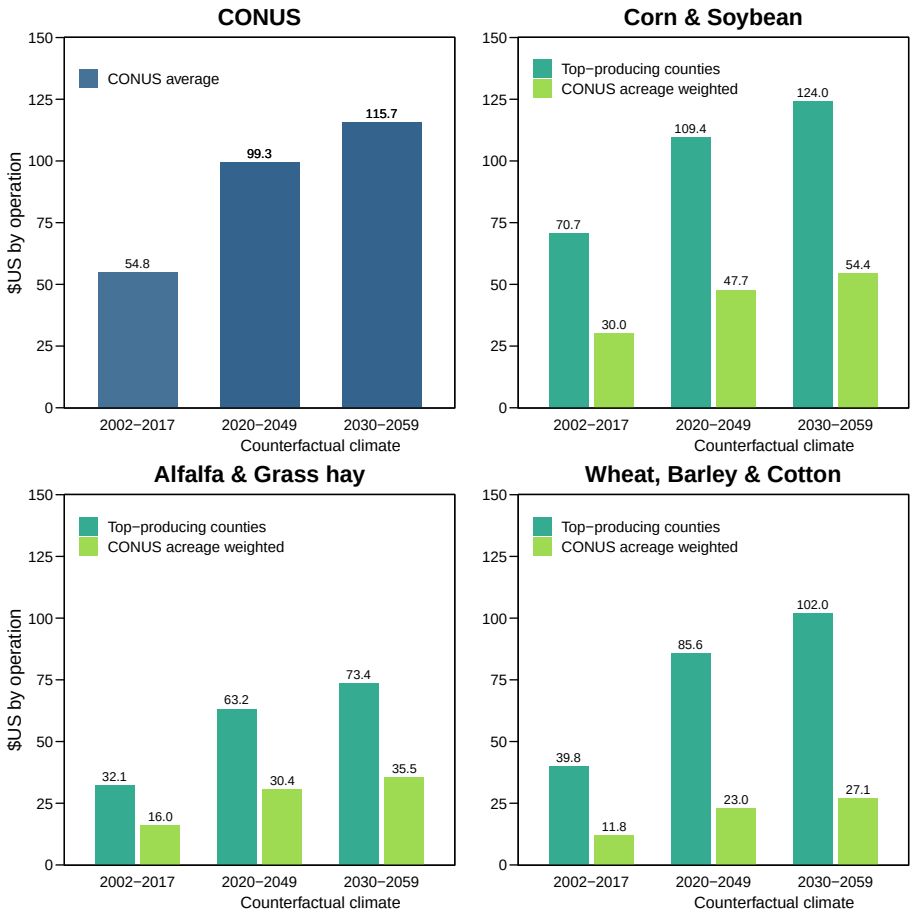

Note: The predicted values of income support payments are similar to those in Figure 5. Projected values on income support payments are based on fixed changes in climate conditions projected with the multi–model ensemble average, while regression coefficients for both net returns' sensitivity to drought and the income–stabilization capacity of income support payments are allowed to take any value within the 95% confidence intervals obtained from non–parametric bootstrapped estimates. The turquoise bars indicate the average predictions for dominant production areas. The green bars show the average predictions weighted by acreage for all cultivated areas across the entire CONUS.

We further analyze the influence of uncertainty on our projected distributions of income support payments, specifically investigating whether the uncertainty is uniformly distributed or confined to observations at the tails of the distribution. Table 6 presents information on the statistical significance of the mean differences between the sample distributions derived from our three sets of projections that account for (a) statistical uncertainty (uncertainty in the regression coefficients), (b)

climate uncertainty (uncertainty in the climate models), and (c) both uncertainties, respectively.[28] By comparing these three distinct sample distributions, we systematically assess the relative contributions of each type of uncertainty to the overall variability in our estimates.

The differences between the sample distributions (b) and (a) indicate that climate uncertainty can significantly impact our average projections of income support payments.[29] The comparison reveals a strongly significant difference in means, even after trimming extreme values, with varying effects depending on the considered crop category. For wheat, barley, and cotton, the comparison of sample distributions between (b) and (a) shows a negative difference in means, indicating that the overall average of distribution after accounting for climate uncertainty is lower than that of distribution after accounting for statistical uncertainty. However, the slightly positive but not significant trimmed mean difference, which excludes extreme values, suggests that the central tendencies of the two distributions are more similar. In contrast, for the other crop categories –corn and soybean, and alfalfa and grass hay–, accounting for climate uncertainty leads to notable differences in the central tendency of our estimates. The comparison between (b) and (a) displays a positive difference in means, with the mean difference becoming even greater and significant after accounting for extreme values. The central tendency between the two distributions is, therefore, different and the difference becomes even more pronounced when considering extreme values.

For all crop categories, the comparison of sample distributions between (c) and (a) shows a difference in means positive and strongly significant, including the trimmed mean difference. The combined effect of both statistical and climate uncertainties leads therefore to a notable difference in central tendency compared to considering only statistical uncertainty (sample distribution a), even after excluding extreme values. Moreover, the combined influence of statistical and climate uncertainties on the overall variability of the estimates is not simply additive. Examining the differences in non–trimmed and trimmed means between our different sets of projections highlights that the cumulative effects of these uncertainties (sample distribution c) cannot be solely explained by the straightforward sum of their individual contributions (sample distributions a and b). This non-additive nature may stem from interactions or synergistic relationships between statistical and climate uncertainties, which in turn cause distinct impacts on the central tendency and distribution of the estimated values when considered together.

[28] To ascertain if extreme values are influencing our overall findings, we calculate the mean differences by incorporating all data points (non-trimmed mean differences) and by excluding the outer 10% of the data as outliers (10% trimmed mean differences), thus providing a more comprehensive statistical assessment of the central tendency in each sample distribution.

[29] See Table D.2 in Appendix D for projected income support payments at the CONUS level and by GCMs.

Table 6: *Robustness of the multi-model ensemble average to the full uncertainty in projecting income support payments for the CONUS and by crop categories, 2030–2059*

	Mean			Mean difference					
	Estimate	CI (95%)			Estimate	Trimmed	Welch t–test[1]		Yuen t–test[2]	
		Lower	Upper				t	p–value	t	p–value
CONUS				**CONUS**						
Regression uncertainty (a)	115.6673	-84.1064	541.4335							
Climate uncertainty (b)	118.8201	-209.4976	427.8468	(b) - (a)	3.1528	15.0215	2.9374***	0.00331	12.973***	0.0000
Total uncertainty (c)	129.2421	-154.3686	646.7052	(c) - (a)	13.5748	13.43136	58.854***	0.00000	56.9265***	0.0000
Corn & Soybean				**Corn & Soybean**						
Regression uncertainty (a)	124.0256	-65.1918	522.3261							
Climate uncertainty (b)	130.7771	-178.9751	481.5001	(b) - (a)	6.7515	15.4723	3.468***	0.0005	7.3651***	0.0000
Total uncertainty (c)	146.0941	-127.2070	787.2290	(c) - (a)	22.0685	15.43128	86.688***	0.0000	62.6179***	0.0000
Alfalfa & Grass hay				**Alfalfa & Grass hay**						
Regression uncertainty (a)	73.40409	-52.4914	358.7091							
Climate uncertainty (b)	78.43444	-122.4318	327.4999	(b) - (a)	5.03035	10.27175	4.004***	0.0000	7.978***	0.0000
Total uncertainty (c)	84.75321	-101.2737	401.9809	(c) - (a)	11.34912	7.5007	69.848***	0.0000	55.529***	0.0000
Wheat, Barley & Cotton				**Wheat, Barley & Cotton**						
Regression uncertainty (a)	101.9669	-69.87284	582.78899							
Climate uncertainty (b)	96.6788	-212.7227	420.9042	(b) - (a)	-5.2901	3.74484	-1.9209*	0.05483	1.3623	0.1841
Total uncertainty (c)	109.1015	-131.1232	706.9986	(c) - (a)	7.1346	3.64616	30.415***	0.0000	17.2671***	0.0000

Note: The estimated mean difference is calculated by comparing: (i) the mean of estimated projections considering climate uncertainty and the mean of estimated projections considering statistical uncertainty (b) – (a) ; (ii) the mean of estimated projections considering total uncertainty and the mean of estimated projections considering statistical uncertainty (c) –(a). The 95% confidence intervals for mean estimates are calculated using the BCa method. [1]We report results from a t–test for mean differences assuming unequal variances between the sampled distributions (Weslsh t–test). [2]We also report the results from a bootstrap trimmed t statistic assuming unequal variance (bootstrapped Yuen t–test) using 1000 repetitions and a trimming factor of 10%. *, **, and *** indicate significance at the 10%, 5% and 1% levels, respectively.

Therefore, our results highlight the importance of considering both statistical and climate uncertainties when analyzing future income support payments related to droughts. Ignoring climate uncertainty may lead to incomplete or potentially biased projections, as considering the full range of climate uncertainty affects the accuracy and reliability of the estimated central tendency, especially in areas producing corn and soybean, and alfalfa and grass hay. Our findings also suggest that the projected increase in support income payments and its associated uncertainty are not necessarily driven by extreme values and may be therefore relatively dispersed across the CONUS. To provide further insights into this issue, we examine the spatial distribution of the projected increase in support income payments.

5.3. Geography of projected income support payments

We calculate the projected payments values at the county level based on the projections for each crop category. Accordingly, we sum up the predictions for all major crops in each county, weighted by the share of cultivated areas. This gives us the total contribution of all major crops to income support payments at the county level. We then multiply our predictions by the number of operations in each county to get the total cost by county. Projected changes are also computed at the county level, by subtracting the projected income support payments from their predicted values. The changes relative to the period 2002–2017 and the total projected income support payments for the 2030–2059 period are shown in Figure 8.

On average, income support payments are expected to increase across all US counties if projected drought conditions over 2030–2059 prevailed. Only three counties localized in Maine should experience a decrease in their income support payments compared to the period 2002–2017. The geographic patterns do not perfectly mirror the geographical distribution of projected future drought conditions (see map B Figure 2). Instead, the largest effects are expected to be in areas that will not necessarily be the driest but where the greatest amount of payments were allocated during the 2002-2017 period. The counties predicted to have the highest increases in costs are mostly concentrated in areas that are currently producing most corn and soybeans, such as the Midwest. Some counties of the Northwest (Oregon, Washington) and the West South Central (Colorado, Texas, Oklahoma) most specialized in wheat, barley, cotton, or alfalfa, and grass hay may also see large increases. The distribution of economic costs offers a similar picture, since large increases in costs are concentrated in areas that received the most payments during the 2002–2017 period, except for counties in the east part of Texas and in Colorado. While these counties are expected to experience significant cost increases, their income support payments are predicted to be lower than those in certain areas of the Midwest, such as Iowa.

Figure 8: *Income support payments under the RCP 8.5 scenario, all major crops, 2030–2059 projections*

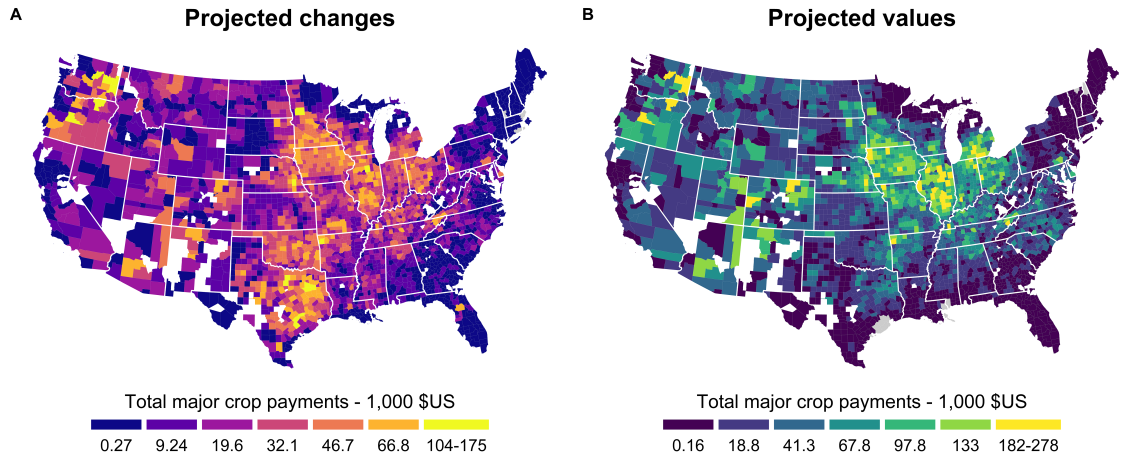

Note: Map A shows the projected levels of income support payments (in 1000 $US 2011 prices) under drought conditions projected for the distant future (2030–2059). Map B shows the projected changes in income support payments between the distant future (2030–2059) and the recent past (2002-2017). We classify data into natural breaks using the Fisher–Jenks algorithm, which clusters data into groups that minimize within–group variance and maximize between–group variance. Counties in grey have negative forecasted values and counties in white color are those that are excluded from our study.

If the United States focuses its agricultural policy on addressing the impact of future droughts, our results suggest that most US counties will need much larger income support payments in the coming decades than in the past. This result provides a strong argument for revising US agricultural policy in a way that could help farmers to better prepare for the coming weather changes in a cost-effective manner. But such revision could also depend on the degree of uncertainty associated with projections of future drought severity and how income support payments can offset income losses caused by drought conditions.

To provide some insights into this issue, we consider the geographic distribution of the total uncertainty surrounding the future path of income support payments. Figure 9 shows two bivariate maps, which combine the predicted variations in income support payments (map A) and their forecasted levels (map B) along with their associated uncertainty.

Figure 9: *Income support payments and uncertainty under the RCP 8.5 scenario, all major crops, 2030–2059 projections*

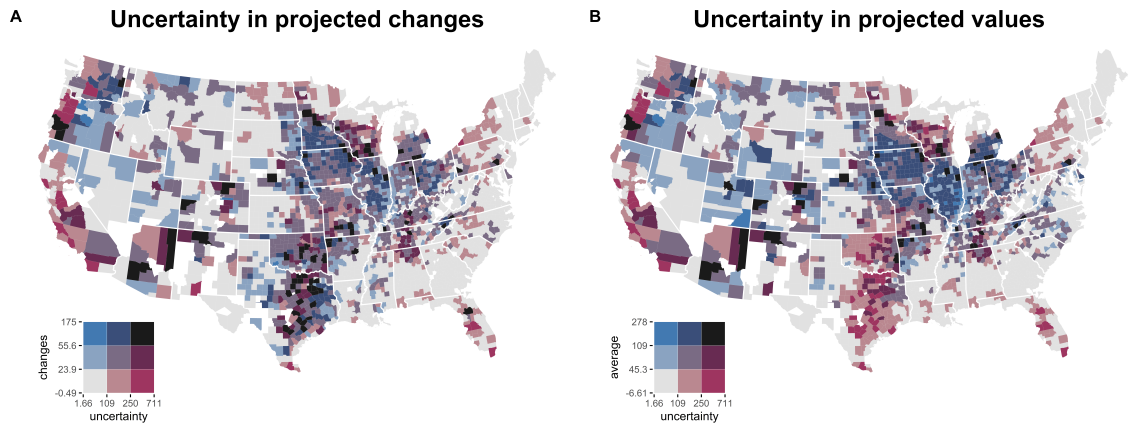

Note: These bivariate maps show forecasted changes in income support payments (map A) and their forecasted values (map B) along with the importance of uncertainty surrounding these forecasts with color–coded legend. The counties with the highest values of forecasted income support payments and low uncertainty are shown in dark blue, while those with high uncertainty are shown in dark purple. We classify data into natural breaks using the Fisher–Jenks algorithm, which clusters data into groups that minimize within–group variance and maximize between–group variance. Counties in white color are those that are excluded from our study.

The two maps show significant differences in the relationship between future income support payments and their associated uncertainty across US counties. Dark blue areas indicate counties where income support payments needed to mitigate drought-induced income losses are expected to be high with low uncertainty. This combination is particularly visible in states such as Wisconsin and Illinois. Drier conditions due to climate change may increase the likelihood of large income losses for farmers in these counties. The implications for program costs are expected to be significant since these counties already receive high income support payments. They also produce crops (corn and soybean) that benefit from payments with a high capacity to mitigate losses in net returns caused by drought conditions. Therefore, for these counties, farm programs should increase the attractiveness of altering current production practices in response to changing climate conditions, so that farmers could better cope with climate change and subsequently decrease the expected cost of climate change in terms of farm income stabilization. In contrast, dark purple areas are characterized by high forecasted income support payments, but with greater uncertainty. This combination is more dispersed over the territory. It occurs in some counties belonging to states along the Pacific coastline of the United States, such as California, Oregon, and Washington. It can also be found in some counties in Midwest states like Missouri and Wisconsin, as well as in West South Central states like Arizona, Oklahoma, and Texas. In these counties with high forecasted income support payments but greater uncertainty, more precise climate change forecasts and improved estimates of income support payments' response are needed. Relative to the group of counties previously

mentioned, less can be said about the severity of future droughts that could threaten agriculture in these geographical areas and the response of income support payments to these threats. As a result, the likelihood of increased costs in the future is also uncertain. Therefore, imposing rigid targets in terms of adaptation strategies in these areas may not be appropriate, since the cost of such policies could be very high, and the benefits in the future uncertain.

In this sense, our results support the major changes made to US agricultural policy since the 2018 Farm Bill and more recently with the Inflation Reduction Act and the USDA's climate-smart commodities partnership, which make climate change a major part of federal farm programs. By considering county-level uncertainty in our assessment of future income support payments, our results also suggest that further exploration is needed to develop policy actions that better account for the uncertainties surrounding the effects of climate change.

6. Conclusion

Since the 1930s, protecting farmers' incomes from market and weather fluctuations has been a major issue in the United States. As such the formal goals of US agricultural policy still reflect this objective with its reference to ensuring a safety net to farmers. However, if climate change increases the severity of droughts and the probability of incurring larger income losses for farmers, this objective could become gradually more costly for US agricultural policy.

In this paper, we quantify these financial costs at the county level for the CONUS and major commodity crops by assessing the future trends of income support payments from expected climate change. Our estimates are based on current US policy design and farmers' behaviors. We extrapolate projected costs from this current environment to a future simulated by climate models. Our findings provide therefore a plausible indirect benchmark for the mid–term cost of adapting to climate change.

We show that income support payments can partially offset losses in net returns caused by drought conditions during the growing season. Our non–parametric estimates confirm that our point estimates are robust and can therefore be used to accurately predict the potential costs of stabilizing farm income due to expected climate change. Using 20 individual climate models under the RCP 8.5 emissions scenario, we predict that droughts across the CONUS will become more severe in the coming decades compared to the recent historical period (1979-2020). Our projections show that the financial cost of stabilizing farm incomes across the CONUS could result in a 111% increase in income support payments compared to the 2002-2017 period if future drought conditions over 2030-2059 prevailed. Even though their contribution to this total cost is expected to decrease, agricultural areas where corn and soybeans are grown should still account for more than 46% of total income support payments.

Our paper also highlights the importance of considering statistical and climate uncertainties when predicting the impact of climate change and identifying which counties are most likely to be impacted. Considering these uncertainties increases the projected financial costs of stabilizing farm income under climate change and reveals two different spatial patterns in areas of high income–stabilizing costs. The first one is centered in Wisconsin and Illinois where the low uncertainty of climate change effects suggests that adaptation measures, as encouraged by recent US agricultural policy changes, are justified, particularly to avoid an increasing trend in income–stabilizing costs. Although the costs of adaptation in these areas may be high today, the benefits of achieving a sustainable trend of income–stabilizing costs in the future could be significant. The other spatial pattern is more dispersed and includes the western parts of Texas and Oklahoma, Wisconsin, and areas along the Pacific coastline. In these areas, uncertainty is more prominent and further research is needed to improve climate change forecasts and estimates of income support payments' response.

While it is beyond the scope of this study to determine specific policy actions that could redesign the US agricultural policy to address uncertainties generated by climate change, our analysis suggests that postponing policy actions until uncertainties are resolved is not an adequate response. Clearly, all climate models project an intensification of droughts in the United States and, despite the uncertainties surrounding our projections, the impacts on income support payments associated with climate change are significant and likely to occur in the near future. These reasons argue for strengthening climate measures in federal government payments to better manage on–farm climate risks and prevent a significant strain on public finances in the coming decades.

References

Abatzoglou, J.T., 2013. Development of gridded surface meteorological data for ecological applications and modelling. International Journal of Climatology 33, 121–131.

Abramowitz, M., Stegun, I.A., 1964. Handbook of Mathematical Functions. U.S. Government printing office.

Ahmadalipour, A., Moradkhani, H., Svoboda, M., 2017. Centennial drought outlook over the CONUS using NASA-NEX downscaled climate ensemble. International Journal of Climatology 37, 2477–2491.

Allen, R.G., Pruitt, W.O., Wright, J.L., Howell, T.A., Ventura, F., Snyder, R., Itenfisu, D., Steduto, P., Berengena, J., Yrisarry, J.B., et al., 2006. A recommendation on standardized surface resistance for hourly calculation of reference ET_0 by the FAO56 Penman-Monteith method. Agricultural Water Management 81, 1–22.

Auffhammer, M., Hsiang, S.M., Schlenker, W., Sobel, A., 2013. Using Weather Data and Climate Model Output in Economic Analyses of Climate Change. Review of Environmental Economics and Policy 7, 181–198.

Barai, K., Tasnim, R., Hall, B., Rahimzadeh-Bajgiran, P., Zhang, Y.J., 2021. Is Drought Increasing in Maine and Hurting Wild Blueberry Production? Climate 9, 178.

Beguería, S., Vicente-Serrano, S.M., Reig, F., Latorre, B., 2014. Standardized precipitation evapotranspiration index (SPEI) revisited: parameter fitting, evapotranspiration models, tools, datasets and drought monitoring. International Journal of Climatology 34, 3001–3023.

Bhaskar, A., Beghin, J.C., 2009. How Coupled Are Decoupled Farm Payments? A Review of the Evidence. Journal of Agricultural and Resource Economics 34, 130–153.

Blanc, E., Schlenker, W., 2017. The Use of Panel Models in Assessments of Climate Impacts on Agriculture. Review of Environmental Economics and Policy 11, 258–279.

Blankenau, P.A., Kilic, A., Allen, R., 2020. An evaluation of gridded weather data sets for the purpose of estimating reference evapotranspiration in the United States. Agricultural Water Management 242, 106376.

Burke, M., Dykema, J., Lobell, D.B., Miguel, E., Satyanath, S., 2015. Incorporating Climate Uncertainty into Estimates of Climate Change Impacts. The Review of Economics and Statistics 97, 461–471.

Burke, M., Emerick, K., 2016. Adaptation to Climate Change: Evidence from US Agriculture. American Economic Journal: Economic Policy 8, 106–140.

Butler, E.E., Huybers, P., 2013. Adaptation of US maize to temperature variations. Nature Climate Change 3, 68–72.

Claassen, R., Aillery, M., Nickerson, C., 2007. Integrating Commodity and Conservation Programs: Design Options and Outcomes. Economic Research Report 44, U.S. Departement of Agriculture.

Crane-Droesch, B., Marshall, E., Rosch, S., Riddle, A., Cooper, J., Wallander, S., et al., 2019. Climate change and agricultural risk management into the 21st century. Economic Research Report 266, U.S. Departement of Agriculture.

Deschênes, O., Greenstone, M., 2007. The Economic Impacts of Climate Change: Evidence from Agricultural Output and Random Fluctuations in Weather. American Economic Review 97, 354–385.

Fisher, A.C., Hanemann, W.M., Roberts, M.J., Schlenker, W., 2012. The Economic Impacts of Climate Change: Evidence from Agricultural Output and Random Fluctuations in Weather: Comment. American Economic Review 102, 3749–3760.

Goodwin, B.K., Mishra, A.K., Ortalo-Magné, F., 2011. The Buck Stops Where? The Distribution of Agricultural Subsidies, in: The Intended and Unintended Effects of US Agricultural and Biotechnology Policies. University of Chicago Press, pp. 15–50.

Hammond Wagner, C.R., Niles, M.T., Roy, E.D., 2019. US county-level agricultural crop production typology. BMC Research Notes 12, 1–3.

Hawkins, E., Sutton, R., 2009. The Potential to Narrow Uncertainty in Regional Climate Predictions. Bulletin of the American Meteorological Society 90, 1095–1108.

Houghton, J., Ding, Y., Griggs, D., Noguer, M., van der Linden, P., Dai, X., Maskell, K., Johnson, C. (Eds.), 2001. IPCC, 2001: Climate Change 2001: The Scientific Basis. Contribution of Working Group I to the Third Assessment Report of the Intergovernmental Panel on Climate Change. Cambridge University Press, Cambridge, United Kingdom and New York, NY, USA, 881pp.

Keane, M., Neal, T., 2020. Climate change and U.S. agriculture: Accounting for multidimensional slope heterogeneity in panel data. Quantitative Economics 11, 1391–1429.

Kharin, V.V., Zwiers, F.W., 2002. Climate Predictions with Multimodel Ensembles. Journal of Climate 15, 793–799.

Kim, J.B., Jiang, Y., Hawkins, L.R., Still, C.J., 2022. A comparison of multiple statistically downscaled climate change datasets for the conterminous USA. Environmental Research Communications 4, 125005.

Knutti, R., Furrer, R., Tebaldi, C., Cermak, J., Meehl, G.A., 2010. Challenges in Combining Projections from Multiple Climate Models. Journal of Climate 23, 2739–2758.

Krakauer, N.Y., Lakhankar, T., Hudson, D., 2019. Trends in Drought over the Northeast United States. Water 11, 1834.

Kuwayama, Y., Thompson, A., Bernknopf, R., Zaitchik, B., Vail, P., 2019. Estimating the Impact of Drought on Agriculture Using the U.S. drought monitor. American Journal of Agricultural Economics 101, 193–210.

Lark, T.J., Schelly, I.H., Gibbs, H.K., 2021. Accuracy, Bias, and Improvements in Mapping Crops and Cropland across the United States Using the USDA Cropland Data Layer. Remote Sensing 13, 968.

Lu, J., Carbone, G.J., Huang, X., Lackstrom, K., Gao, P., 2020. Mapping the sensitivity of agriculture to drought and estimating the effect of irrigation in the United States, 1950–2016. Agricultural and Forest Meteorology 292, 108124.

McIntosh, C.T., Schlenker, W., 2006. Identifying Non-linearities in Fixed-Effects Models. Technical Report. UC-San Diego Working Paper, University California San Diego.

McKee, T.B., Doesken, N.J., Kleist, J., 1995. Drought Monitoring with Multiple Time Scales, in: Proceedings of 9th Conference on Applied Climatology, The Society. pp. 233–236.

Mishra, A.K., Singh, V.P., 2010. A review of drought concepts. Journal of Hydrology 391, 202–216.

Palmer, W.C., 1965. Meteorological drought. volume 30. US Department of Commerce, Weather Bureau.

Peel, M.C., Finlayson, B.L., McMahon, T.A., 2007. Updated world map of the Köppen–Geiger climate classification. Hydrology and Earth System Sciences 11, 1633–1644.

Peña-Gallardo, M., Vicente-Serrano, S.M., Quiring, S., Svoboda, M., Hannaford, J., Tomas-Burguera, M., Martín-Hernández, N., Domínguez-Castro, F., El Kenawy, A., 2019. Response of crop yield to different time-scales of drought in the United States: Spatio-temporal patterns and climatic and environmental drivers. Agricultural and Forest Meteorology 264, 40–55.

Peng, P., Kumar, A., van den Dool, H., Barnston, A.G., 2002. An analysis of multimodel ensemble predictions for seasonal climate anomalies. Journal of Geophysical Research: Atmospheres 107, ACL–18.

Pörtner, H.O., Roberts, D.C., Adams, H., Adler, C., Aldunce, P., Ali, E., Begum, R.A., Betts, R., Kerr, R.B., Biesbroek, R., et al., 2022. Climate change 2022: Impacts, Adaptation and Vulnerability. IPCC Geneva, Switzerland.

Ramcharan, R., 2010. Inequality and Redistribution: Evidence from U.S. Counties and States, 1890–1930. The Review of Economics and Statistics 92, 729–744.

Reidmiller, D., Avery, C., Easterling, Kunkel, D.K., Lewis, K., Maycock, T., Stewart, B., 2018. Impacts, Risks, and Adaptation in the United States: Fourth National Climate Assessment (NCA4), volume II. U.S. Global Change Research Program, Washington, DC, USA, 1515 pp. .

Rippey, B.R., 2015. The US drought of 2012. Weather and Climate Extremes 10, 57–64.

Roberts, M.J., Schlenker, W., 2011. Is Agricultural Production Becoming More or Less Sensitive to Extreme Heat? Evidence from U.S. Corn and Soybean Yields, in: Fullerton, D., Wolfram, C. (Eds.), The Design and Implementation of US Climate Policy. University of Chicago Press, pp. 271–282.

Rodziewicz, D., Dice, J., 2020. Drought Risk to the Agriculture Sector. Economic Review (01612387) 105.

Santini, M., Noce, S., Antonelli, M., Caporaso, L., 2022. Complex drought patterns robustly explain global yield loss for major crops. Scientific Reports 12, 5792.

Schlenker, W., Michael Hanemann, W., Fisher, A.C., 2005. Will U.S. Agriculture Really Benefit from Global Warming? Accounting for Irrigation in the Hedonic Approach. American Economic Review 95, 395–406.

Schlenker, W., Roberts, M.J., 2009. Nonlinear temperature effects indicate severe damages to U.S. crop yields under climate change. Proceedings of the National Academy of Sciences 106, 15594–15598.

Schwalm, C.R., Glendon, S., Duffy, P.B., 2020. RCP8.5 tracks cumulative CO_2 emissions. Proceedings of the National Academy of Sciences 117, 19656–19657.

Shepherd, T.G., 2014. Atmospheric circulation as a source of uncertainty in climate change projections. Nature Geoscience 7, 703–708.

Tack, J., Barkley, A., Nalley, L.L., 2015. Effect of warming temperatures on US wheat yields. Proceedings of the National Academy of Sciences 112, 6931–6936.

Tam, B.Y., Szeto, K., Bonsal, B., Flato, G., Cannon, A.J., Rong, R., 2019. Cmip5 drought projections in Canada based on the Standardized Precipitation Evapotranspiration Index. Canadian Water Resources Journal/Revue canadienne des ressources hydriques 44, 90–107.

Taylor, K.E., 2001. Summarizing multiple aspects of model performance in a single diagram. Journal of Geophysical Research: Atmospheres 106, 7183–7192.

Tebaldi, C., Knutti, R., 2007. The use of the multi-model ensemble in probabilistic climate projections. Philosophical Transactions of the Royal Society A: Mathematical, Physical and Engineering Sciences 365, 2053–2075.

Tian, L., Yuan, S., Quiring, S.M., 2018. Evaluation of six indices for monitoring agricultural drought in the south-central United States. Agricultural and Forest Meteorology 249, 107–119.

Vicente-Serrano, S.M., Beguería, S., López-Moreno, J.I., 2010. A Multiscalar Drought Index Sensitive to Global Warming: The Standardized Precipitation Evapotranspiration Index. Journal of Climate 23, 1696–1718.

Weber, J.G., Key, N., 2012. How much Do Decoupled Payments Affect Production? An Instrumental Variable Approach with Panel Data. American Journal of Agricultural Economics 94, 52–66.

Westcott, P.C., Young, C.E., 2004. Farm Program Effects on Agricultural Production: Coupled and Decoupled Programs, in: Burfisher, M.E., Hopkins, J. (Eds.), Decoupled Payments in a Changing Policy Setting. U.S. Department of Agriculture. chapter 1, pp. 7–17.

Wuebbles, D., Fahey, D., Takle, E., Hibbard, K., Arnold, J., DeAngelo, B., Doherty, S., Easterling, D., Edmonds, J., Edmonds, T., et al. (Eds.), 2017. Climate Science Special Report: Fourth National Climate Assessment (NCA4), Volume I. U.S. Global Change Research Program, Washington, DC, USA, 470 pp.

Yaddanapudi, R., Mishra, A.K., 2022. Compound impact of drought and COVID-19 on agriculture yield in the USA. Science of the Total Environment 807, 150801.

Zipper, S.C., Qiu, J., Kucharik, C.J., 2016. Drought effects on US maize and soybean production: spatiotemporal patterns and historical changes. Environmental Research Letters 11, 094021.

Appendix A. Multi–model ensemble average validation

We check the accuracy of our results, which are calculated by taking the average of 20 individual GCMs (MME average). We do this by assessing the level of agreement between each downscaled GCM, including the MME average, and observations from the gridMET dataset over the reference period of 1979–2020. Specifically, we apply the Taylor diagram (Taylor, 2001), which simultaneously represents three different statistics: the centered root mean square (RMS) difference, the Pearson correlation, and the standard deviation. This approach allows us to determine if the MME average outperforms individual GCM simulations in reproducing weather patterns for each county in the CONUS. The performance evaluation is conducted for three variables (precipitation, evapotranspiration, and water balance) on a monthly basis over the period 1979-2020, which represent a total of 1,566,462 observations for each model. We also use the root mean square error (RMSE), the mean absolute error (MAE), and the coefficient of determination R-squared (R^2) as additional statistical metrics to measure the performance of the models. The main results of this performance evaluation are presented in Figure A.1.

Figure A shows that the MME average has a pattern correlation of 0.62 with gridMET reanalysis data for precipitation from 1979-2020 across the CONUS. Individual GCMs, on the other hand, have a lower level of agreement with observations as they are less able to reproduce inter–monthly variations in precipitation. Figures B and C show that the MACA v2 dataset has excellent statistical properties for describing historical temperatures used to calculate reference evapotranspiration and the climatic water balance. The correlation between the MME average and observations is 0.95 for reference evapotranspiration and 0.72 for water balance. Taylor diagrams also show that the MME average underestimates the standard deviations in precipitation and water balance due to error compensations in individual downscaled GCMs. Bias analysis (Figure D) also confirms that the MME average performs well in reproducing observed weather patterns. The normalized mean absolute biases are less than 3% for all variables used to calculate the drought index and are much lower than those of individual models. Table A.1 details the 20 downscaled GCMs in the MACA v2 dataset. Table A.2 provides more details on the performance metrics.

Figure A.1: *Performance evaluation of the multi–model ensemble average (MME) and 20 downscaled GCMs over the reference period 1979-2020*

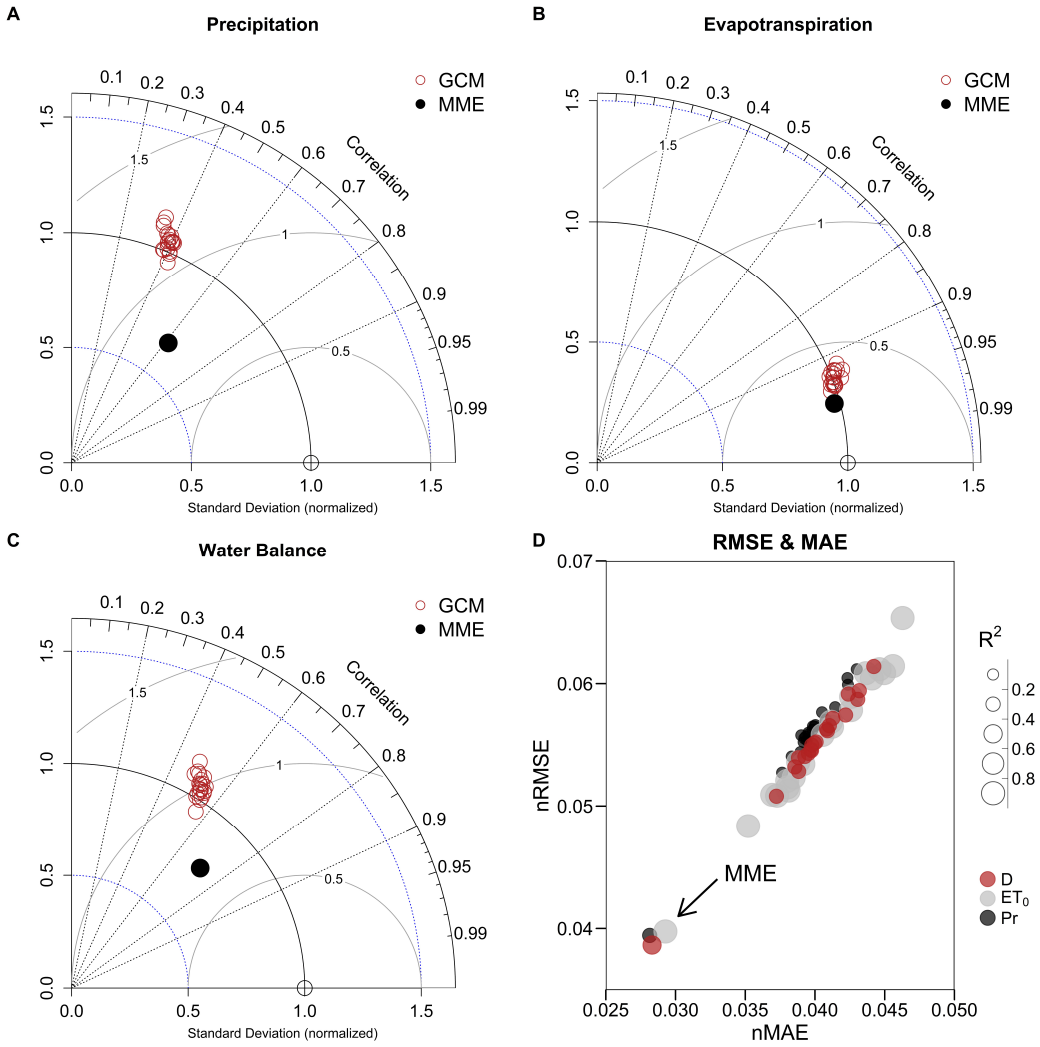

Note: Taylor diagrams compare the climatological mean for the reference period 1979-2020 of the multi–model ensemble average (black solid circle) and each downscaled GCM (red circle) to US gridded observations from gridMET (black circle, circle at 1.0 on the x–axis of the graphs). The standard deviation is shown by the distance from gridMET observations. The root–mean–square difference between each model, including the multi–model ensemble average, and observations is shown by the circular contours centered on the gridMET data point. The correlation between model data and observations is shown by the azimuthal angle (straight lines from the origin). Figure D shows measures of average error magnitudes, including the root–mean–square error (RMSE), the mean absolute error (MAE), and the R^2. The RMSE is the square root of the variance of the residuals or the square root of the mean square error (MSE), which measures the average of the squared deviations between the fitted values and the actual data observations. The R^2 value measures how much of the variation is accounted for by the fitted model.

Table A.1: *20 GCMs used in this study and their characteristics*

Model Name	Country	Model Agency	Resolution	Ensemble
bcc–csm1–1	China	Beijing Climate Center, China Meteorological Association	$2.80° \times 2.80°$	r1i1p1
bcc–csm1–1–m	China	Beijing Climate Center, China Meteorological Association	$1.12° \times 1.12°$	r1i1p1
BNU–ESM	China	College of Global Change and Earth System Science, China	$2.80° \times 2.80°$	r1i1p1
CanESM2	Canada	Canadian Center for Climate Modeling and Analysis	$2.80° \times 2.80°$	r1i1p1
CCSM4	USA	National Center of Atmospheric Research	$1.25° \times 0.94°$	r6i1p1
CNRM–CM5	France	National Center of Meteorological Research	$1.40° \times 1.40°$	r1i1p1
CSIRO–Mk3–6–0	Australia	Commonwealth Scientific and Industrial Research Organization	$1.80° \times 1.80°$	r1i1p1
GDFL–ESM2M	USA	NOAA Geophysical Fluid Dynamics Laboratory	$2.50° \times 2.00°$	r1i1p1
GDFM–ESM2G	USA	NOAA Geophysical Fluid Dynamics Laboratory	$2.50° \times 2.00°$	r1i1p1
HadGEM2–ES	UK	Met Office Hadley Center	$1.88° \times 1.25°$	r1i1p1
HadGEM2–CC	UK	Met Office Hadley Center	$1.88° \times 1.25°$	r1i1p1
inmcm4	Russia	Institute for Numerical Mathematics	$2.00° \times 1.50°$	r1i1p1
IPSL–CM5A–LR	France	Institut Pierre Simon Laplace	$3.75° \times 1.80°$	r1i1p1
IPSL–CM5A–MR	France	Institut Pierre Simon Laplace	$2.50° \times 1.25°$	r1i1p1
IPSL–CM5B–LR	France	Institut Pierre Simon Laplace	$2.75° \times 1.80°$	r1i1p1
MIROC5	Japan	Japan Agency for Marine-Earth Science and Technology	$1.40° \times 1.40°$	r1i1p1
MIROC–ESM	Japan	Japan Agency for Marine-Earth Science and Technology	$2.80° \times 2.80°$	r1i1p1
MIROC–ESM–CHEM	Japan	Japan Agency for Marine-Earth Science and Technology	$2.80° \times 2.80°$	r1i1p1
MRI–CGCM3	Japan	Meteorological Research Institute, Japan	$1.10° \times 1.10°$	r1i1p1
NorESM1–M	Norway	Norwegian Climate Center, Norway	$2.50° \times 1.90°$	r1i1p1

Note: Table A.1 reports the downscaled GCMs chosen for this study and their main characteristics. This selection was based on the maximum number of models forced by the same GCMs. Source: https://climate.northwestknowledge.net/MACA/GCMs.php

Table A.2: *Performance metrics by downscaled GCMs including the multi–model ensemble average (MME)*

	Normalized Mean Absolute Error			Normalized Mean Bias			Normalized Root Mean Square Error			R^2		
Model	Pr	ET_0	D	Pr	ET_0	D	Pr	ET_0	D	Pr	ET_0	D
Bcc-csm1-1	0.040781	0.044955	0.042197	-0.00126136	-0.00082126	-0.00090014	0.05704630	0.06086045	0.05744399	0.1520289	0.8604849	0.2680627
Bcc-csm1-1-m	0.041446	0.045596	0.043062	-0.00042355	-0.00375409	0.00051058	0.05808160	0.06143429	0.05871830	0.1377022	0.8583235	0.2474646
BNU-ESM	0.039534	0.040546	0.039964	-0.00105225	0.00265706	-0.00153987	0.05599248	0.05581723	0.05514686	0.1594757	0.8844807	0.2918692
CNRM-CM5	0.039237	0.042586	0.040081	-0.00035919	-0.00573455	0.00103242	0.05553510	0.05784373	0.05524121	0.1668787	0.8709919	0.2789683
CSIRO-Mk3-6-0	0.039336	0.044624	0.040825	-0.00267230	0.00250565	-0.00289612	0.05567131	0.06117986	0.05629071	0.1445330	0.8651013	0.2747759
GDFL-ESM2M	0.040029	0.044079	0.041031	0.00038143	-0.00684107	0.00192942	0.05662157	0.06042377	0.05657094	0.1513044	0.8617753	0.2651352
GDFL-ESM2G	0.039964	0.042589	0.040893	-0.00098110	-0.00259604	-0.00024126	0.05651403	0.05892759	0.05615892	0.1488542	0.8680112	0.2708258
HadGEM2-CC	0.042365	0.043637	0.043178	-0.00218707	0.00161485	-0.00226938	0.05990555	0.06085139	0.05942279	0.1219232	0.8622871	0.2394922
HadGEM2-ES	0.042995	0.046281	0.044220	-0.00072638	0.00176039	-0.00104865	0.06117036	0.06535305	0.06139411	0.1200920	0.8438828	0.2291346
CanESM2	0.042328	0.038029	0.042390	-0.00062642	-0.00127369	-0.00024803	0.06045387	0.05154085	0.05914802	0.1193810	0.8962452	0.2340431
CCSM4	0.039536	0.038007	0.039536	-0.00030466	-0.00056543	-0.00013843	0.05584266	0.05207922	0.05431351	0.1630718	0.8947726	0.2958582
NorESM1-M	0.039015	0.036929	0.038819	0.00015471	-0.00132872	0.00043607	0.05578931	0.05092814	0.05395873	0.1617085	0.8989908	0.2986299
Inmcm4	0.040505	0.041148	0.041276	-0.00167613	-0.00377422	-0.00056087	0.05766492	0.05689389	0.05716825	0.1427072	0.8758327	0.2638425
IPSL-CM5A-LR	0.039822	0.038108	0.039710	-0.00193737	0.00024814	-0.00173287	0.05622682	0.05127471	0.05461361	0.1498003	0.8978764	0.2837399
IPSL-CM5A-MR	0.039854	0.037282	0.039768	-0.00182082	-0.00148555	-0.00122433	0.05651441	0.05085956	0.05498061	0.1493531	0.8992345	0.2828327
IPSL-CM5B-LR	0.038966	0.038473	0.038830	-0.00120755	-0.00273106	-0.00040401	0.05441932	0.05235047	0.05284211	0.1662510	0.8924216	0.3014725
MIROC5	0.039187	0.038794	0.039274	-0.00054731	-0.00103295	-0.00023677	0.05523243	0.05360190	0.05406150	0.1559029	0.8879327	0.2812862
MIROC5-ESM	0.038329	0.039164	0.038560	-0.00143846	-0.00332274	-0.00046302	0.05405203	0.05343946	0.05320561	0.1685030	0.8896251	0.3014773
MIROC5-CHEM	0.039420	0.041223	0.039751	-0.00061468	-0.00333463	0.00024755	0.05538665	0.05648318	0.05454454	0.1477985	0.8777419	0.2793681
MRI-CGCM3	0.037641	0.035205	0.037236	-0.00143860	-0.00609916	0.00019089	0.05274010	0.04835031	0.05081201	0.1747659	0.9085810	0.3147745
MME	0.028148	0.029270	0.028315	-0.00103695	-0.00179545	-0.00047784	0.03943045	0.03975445	0.03865439	0.3768876	0.9370007	0.5184420

Note: Pr, ET_0, D, stand for precipitation, evapotranspiration, and water balance, respectively.

Figure A.2: *Geographical distribution of the layers w_i for the years 2008, 2012, and 2017*

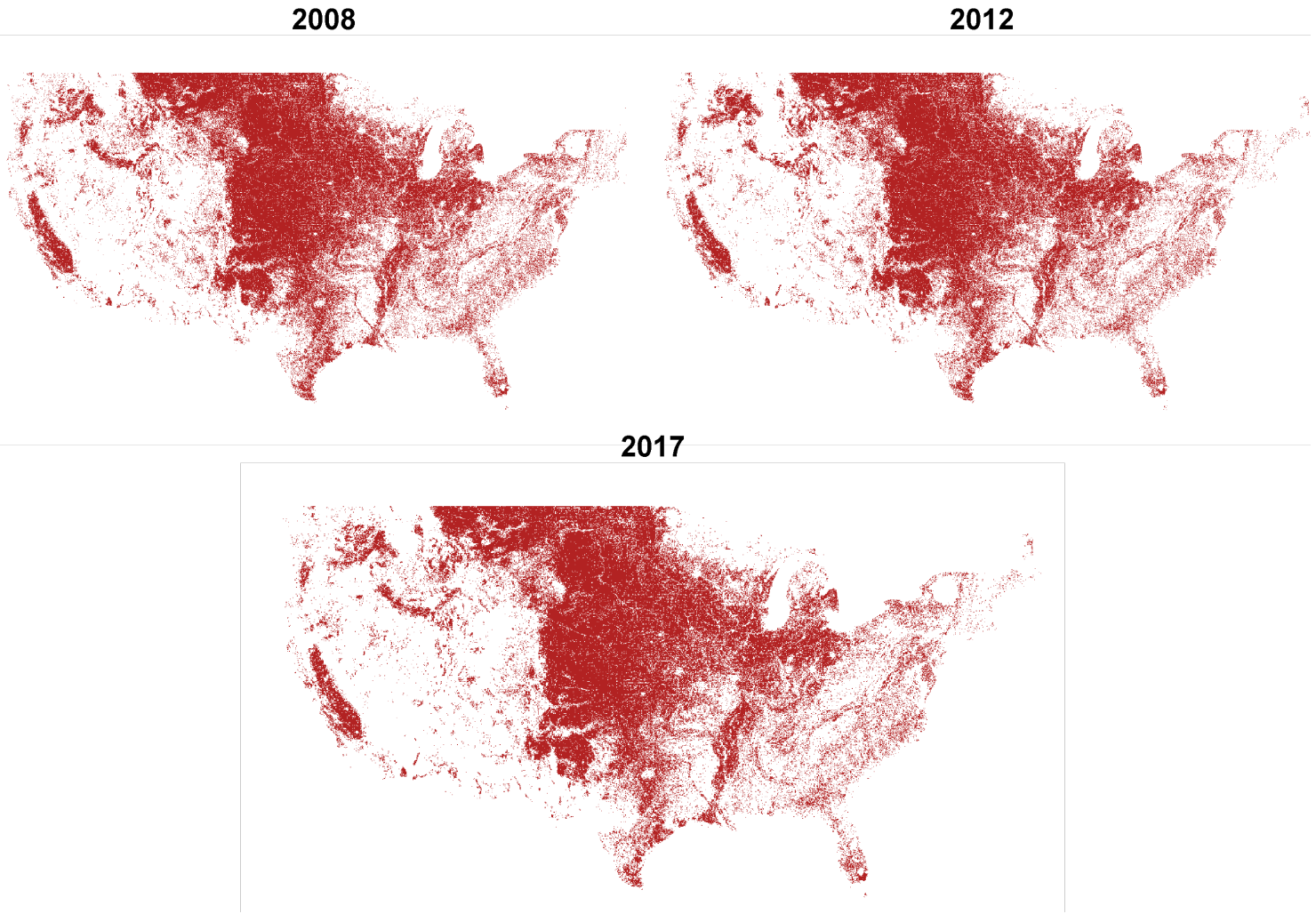

Note: Figure A.2 displays the geographical distribution of the layers w_i for the years 2008, 2012, and 2017. The layer is assigned a value of 1 if there is at least one parcel present within each SPEI data grid and a missing value otherwise.

Figure A.3: *Crop calendars for the United States*

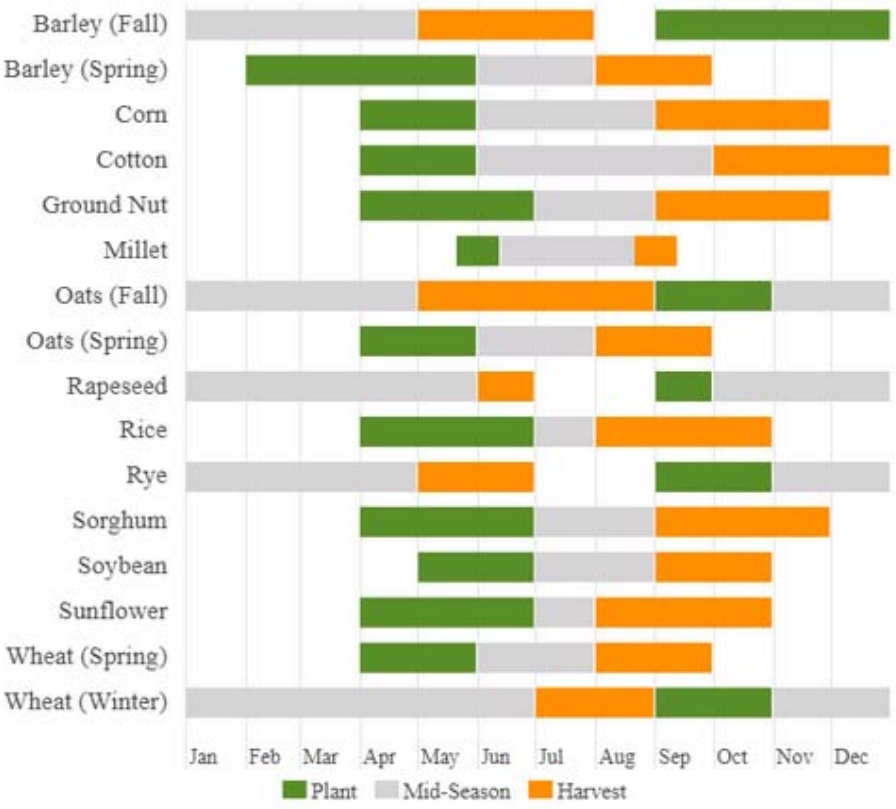

Source: US Department of Agriculture. https://ipad.fas.usda.gov/rssiws/al/crop_calendar/us.aspx

Appendix B. SPEI methodology

The SPEI uses, as its input, a "climatic water balance" calculated as the difference between precipitation and reference evapotranspiration.[30] By relying on the combined effects of precipitation and reference evapotranspiration, this index better accounts for the impact of surface warming on droughts and wet spells compared to other drought indices. In this paper, reference evapotranspiration refers to the ASCE Penman–Monteith (ASCEPM) formulation, as recommended by the United Nations Food and Agriculture Organization (FAO).[31] The Penman–Monteith reference evapotranspiration (ET_0) is formulated as:

$$ET_0 = \frac{0.408\Delta(R_n - G) + \gamma \frac{900}{T+273} u_2 (e_a - e_d)}{\Delta + \gamma(1 + 0.34u_2)} \tag{B.1}$$

Where Δ is the slope of the saturation vapor pressure function of temperature in $kPa^{\circ}C^{-1}$, R_n is the net radiation in $MJm^{-2}d^{-1}$, G is soil heat flux in $MJ.m^{-}2.d^{-1}$, γ is the psychrometric constant in $kPa^{\circ}C^{-1}$, T is the mean surface temperature in °C, u_2 is the wind speed at 2m above the surface in $m.s^{-1}$, and e_a and e_d are the saturation and actual vapor pressure in kPa, respectively.

We aggregate daily precipitation (Pr) and reference evapotranspiration (ET_0) data on a monthly basis to obtain monthly time–series climatic water balance (D_m) for each pixel from January 1979 to December 2020.[32]

$$D_m = Pr_m - ET_{0,m} \tag{B.2}$$

To calculate the SPEI, we use a three–step process (Vicente-Serrano et al., 2010). The first step involves accumulating water balance series at different time scales. In this study, we use a 3–month timescale, which is most appropriate for identifying drought impacts on crop yields (Santini et al., 2022; Peña-Gallardo et al., 2019). The cumulative water balance for a month m in a particular year t based on a 3–month timescale is calculated as follows:

$$X_{t,m}^{k=3} = \begin{cases} \sum_{l=13-k+m}^{12} D_{t-1,l} + \sum_{l=1}^{m} D_{t,l}, & \text{if } m < k \\ \sum_{l=m-k+1}^{m} D_{t,l}, & \text{if } m \geq k \end{cases} \tag{B.3}$$

[30] Reference evapotranspiration is the estimation of the evapotranspiration from the "reference surface". The reference surface is a hypothetical grass reference crop with an assumed crop height of 0.12 m, a fixed surface resistance of 70 s/m and an albedo of 0.23. The reference surface closely resembles an extensive surface of green, well–watered grass of uniform height, actively growing and completely shading the ground.

[31] This formulation has a more physically robust calculation process than other standard formulations provided by the Hargreaves or the Thornthwaite equations.

[32] The period 1979–2020 is the reference period (i.e., calibration period). Estimating a drought index requires a sufficiently long base period (30–40 years) that samples the natural variability to describe average conditions and associated anomalies.

Where $X_{t,m}^{k=3}$ is the accumulated difference between precipitation (Pr) and reference evapotranspiration (ET_0) at the k-month time scale in the m^{th} month of year t. $D_{t,l}$ is the monthly difference between precipitation (Pr) and reference evapotranspiration (ET_0) in the l^{th} month of year t.

The second step involves normalizing the accumulated water balance series $X_{t,m}^{k=3}$ at each grid cell. This normalization is necessary due to seasonal differences in precipitation and evapotranspiration and the heterogeneity of climate regimes. The data series is transformed to a normal distribution with a mean of zero and a standard deviation of one using equal probability. As suggested by Vicente-Serrano et al. (2010) a three–parameter log–logistic probability distribution is used to fit the data due to the presence of negative values in the original data sequence. Estimating the parameters of the log-logistic probability distribution is essential for accurate drought analysis and monitoring. This allows for spatial and temporal comparisons of the SPEI series at different locations, which must have the same average of zero and standard deviation equal to unity. The accumulative function of the log–logistic probability distribution $F(X)$ is given by:

$$F(X) = \left[1 + \left(\frac{\alpha}{X - \gamma}\right)^{\beta}\right]^{-1} \tag{B.4}$$

α, β, and γ represent the scale, shape and origin parameters respectively that are estimated from the sample X (difference between precipitation and ET_0).

The final step involves deriving the SPEI values from the standardized values of the cumulative function of the log-logistic probability distribution $F(X)$. This is done using the approximation method of Abramowitz and Stegun (1964):

$$SPEI = \frac{W - (C_0 + C_1 W + C_2 W^2)}{1 + d_1 W + d_2 W^2 + d_3 W^3} \tag{B.5}$$

Where $W = \sqrt{-2\ln(P)}$ for $P \leq 0.5$ with $P = 1 - F(X)$, the probability of exceeding a determined D value. The constants are $C_0 = 2.515517$, $C_1 = 0.802853$, $C_2 = 0.010328$, $d_1 = 1.432788$, $d_2 = 0.189269$ and $d_3 = 0.001308$.

By doing so, the values of the SPEI are in standard deviations from a long–term mean centered around zero and are comparable in space and time.[33] The long–term mean represents the typical climate at each cell during a reference period (in this case, 1979–2020). Negative values indicate a deficit in the water balance, i.e., drier conditions than the typical climate, and positive values denote wetness in excess of normal conditions.

[33]The parameters of these density functions were obtained by the method of unbiased probabilistic weighted moments, which is recommended over other methods (Beguería et al., 2014).

Following Tam et al. (2019), the calculation of future drought conditions over the CONUS requires two steps. First, we calculate monthly climate balance series from 1979 to 2100 for each downscaled GCM f ($f = 1, \ldots, 20$) and for the multi–model ensemble (MME) average:

$$D_m^f = Pr_m^f - ET_{0,m}^f \tag{B.6}$$

$$D_m^{MME} = Pr_m^{MME} - ET_{0,m}^{MME} \tag{B.7}$$

Where Pr_m^{MME} and $ET_{0,m}^{MME}$ correspond respectively to the average over time of precipitation and reference evapotranspiration of the 20 individual downscaled GCMs. The resulting projections for the historical period are used to evaluate the performance of each GCM compared to actual observations.

Second, the calculation of future SPEI, $SPEI_m^f$ and $SPEI_m^{MME}$, is done by fitting the accumulated D_m^f and D_m^{MME} values on a 3–month timescale to the log–logistic model, using distribution coefficients established from observed D_m for the 1979–2020 reference period (Eq. B.4). Projected drought conditions at a location are expressed as the number of standard deviations by which the future SPEI deviates from its mean value for the 1979–2020 reference period. Since the SPEI is a z–score with zero mean over the reference period, a projected SPEI value of zero indicates no change in drought conditions relative to the reference period.

Appendix C. Empirical framework

Table C.1: *Summary statistics, control variables, CONUS*

Census years	2002	2007	2012	2017
Mean share of irrigated land in total agricultural land (%)	3.061	3.212	3.236	3.413
Median share of irrigated land in total agricultural land (%)	0.375	0.377	0.358	0.383
Mean share of cropland in total agricultural land (%)	52.465	51.532	51.049	50.368
Median share of cropland in total agricultural land (%)	50.832	48.767	48.237	46.865
Average median farm size	220.187	190.780	193.412	191.308

Note: All variables are measured in acres and calculated per operation. Source: Census of Agriculture.

Table C.2: *Robustness Check, CONUS average, 2002–2017*

	Benchmark results		Including lagged SPEI		Placebo test			
					Non-metropolitan counties		Metropolitan counties	
	1st stage	2nd stage	1st stage	2nd stage	1st stage	2nd stage	1st stage	2nd stage
	(1)	(2)	(3)	(4)	(5)	(6)	(7)	(8)
Dry	-0.0071***		-0.0070***		-0.0097***		-0.0015	
	(0.0013)		(0.0013)		(0.0017)		(0.0019)	
Dry(-1)			-0.0014					
			(0.0010)					
Inc		-0.3569***		-0.3231***		-0.3489***		0.3517
		(0.1260)		(0.1202)		(0.1141)		(0.8537)
Irrigation	0.0038***	0.0014*	0.0038***	0.0013*	0.0033***	0.0008	0.0023	-0.0005
	(0.0009)	(0.0008)	(0.0009)	(0.0007)	(0.0011)	(0.0008)	(0.0015)	(0.0021)
Field crop	0.0317***	0.0280***	0.0318***	0.0269***	0.0183*	0.0266***	0.0369**	-0.0098
	(0.0089)	(0.0059)	(0.0089)	(0.0057)	(0.0102)	(0.0063)	(0.0163)	(0.0346)
Concentration	0.0145**	0.0358***	0.0146**	0.0353***	0.0154**	0.0397***	0.0111	0.0060
	(0.0060)	(0.0048)	(0.0060)	(0.0046)	(0.0068)	(0.0057)	(0.0125)	(0.0092)
N		9607		9607		7164		2443
F-stat		17.886		19.062		15.690		0.7261
KP F-stat		27.827		13.914		33.100		0.6420
KP-LM test		27.390***		27.419***		32.598***		0.6394
Hansen J				2.494				
Hansen J p-val				0.114				

Note: The excluded instrument is the drought index (equation 1). A rise in this index reflects drier conditions. *, **, and *** indicate significance at the 10%, 5% and 1% levels, respectively. The first-stage F-stat is used to investigate the strength of the instruments. The Kleibergen and Paap Wald rk F–stat test if the excluded instruments are weak (weak identification). The null hypothesis of the Kleibergen–Paap rk LM–stat, KP LM–stat, is that the equation is underidentified. Hansen's J test for exogeneity (in case of more instruments than endogenous variables). Robust standard errors clustered by Federal Information Processing System (FIPS) codes are reported in brackets.

Table C.3: *Alternative measure of the drought index, CONUS average, 2002–2017*

	Benchmark results		Including lagged PDSI		Placebo test			
					Non-metropolitan counties		Metropolitan counties	
	1st stage	2nd stage	1st stage	2nd stage	1st stage	2nd stage	1st stage	2nd stage
	(1)	(2)	(3)	(4)	(5)	(6)	(7)	(8)
PDSI	0.0021***		0.0019***		0.0028***		0.0010*	
	(0.0004)		(0.0004)		(0.0005)		(0.0006)	
PDSI(-1)			0.0007**					
			(0.0003)					
Inc		-0.3338***		-0.1668*		-0.2944***		-0.3290
		(0.1168)		(0.0976)		(0.1057)		(0.4054)
Irrigation	0.0038***	0.0013*	0.0038***	0.0007	0.0034***	0.0006	0.0025*	0.0010
	(0.0009)	(0.0007)	(0.0009)	(0.0006)	(0.0011)	(0.0007)	(0.0015)	(0.0013)
Field crop	0.0323***	0.0272***	0.0330***	0.0218***	0.0194*	0.0256***	0.0368**	0.0155
	(0.0089)	(0.0057)	(0.0089)	(0.0049)	(0.0102)	(0.0060)	(0.0165)	(0.0173)
Concentration	0.0146**	0.0354***	0.0145**	0.0330***	0.0157**	0.0389***	0.0109	0.0134**
	(0.0060)	(0.0045)	(0.0060)	(0.0040)	(0.0068)	(0.0054)	(0.0124)	(0.0061)
N		9607		9607		7164		2443
F–stat		19.275		21.34		20.05		0.2452
KP F–stat		30.458		16.839		34.328		2.926
KP–LM test		30.301***		33.594***		34.168***		2.921*
Hansen J				22.910				

Note: The excluded instrument is the PDSI developed by Palmer (1965). Positive (negative) PDSI values represent wet (dry) conditions. *, **, and *** indicate significance at the 10%, 5% and 1% levels, respectively. The first-stage F–stat is used to investigate the strength of the instruments. The Kleibergen and Paap Wald rk F–stat test if the excluded instruments are weak (weak identification). The null hypothesis of the Kleibergen-Paap rk LM–stat, KP LM–stat, is that the equation is underidentified. Hansen's J test for exogeneity (in case of more instruments than endogenous variables). Robust standard errors clustered by Federal Information Processing System (FIPS) codes are reported in brackets.

Table C.4: *Spearman's rank correlation test results*

	Corn grain	Soybeans	Hay	Wheat	Barley	Cotton
Corn grain	1	0.779***	-0.623***	0.070***	0.019**	-0.092***
Soybeans		1	-0.059***	0.129***	-0.064***	-0.017*
Hay			1	-0.326***	-0.037***	-0.210***
Wheat				1	0.282***	0.290***
Barley					1	-0.237***
Cotton						1

Note: *, **, and *** indicate significance at the 10%, 5% and 1% levels, respectively.

Appendix D. Climate projections

Table D.1: *Future severity of droughts (as deviations from the reference period of 1979–2020) by downscaled GCMs, including the multi–model ensemble average (MME), under the RCP 8.5 scenario, CONUS average*

Downscaled GCMs	2020-2049	2030-2059
HadGEM2–ES	+0.558	+0.703
HadGEM2–CC	+0.444	+0.502
IPSL–CM5A–MR	+0.346	+0.461
NorESM1–M	+0.352	+0.415
CCSM4	+0.303	+0.439
IPSL–CM5A–LR	+0.273	+0.382
MIROC5	+0.257	+0.371
MIROC5–CHEM	+0.241	+0.376
Bcc–csm1–1–m	+0.213	+0.341
MME	**+0.224**	**+0.306**
Bcc–csm1–1	+0.187	+0.341
CanESM2	+0.249	+0.267
MIROC5–ESM	+0.216	+0.276
BNU–ESM	+0.183	+0.302
Inmcm4	+0.110	+0.260
CSIRO–Mk3–6–0	+0.194	+0.159
IPSL–CM5B–LR	+0.170	+0.153
CNRM–CM5	+0.126	+0.172
MRI–CGCM3	+0.013	+0.019
GDFL–ESM2G	-0.001	+0.107
GDFL–ESM2M	-0.027	+0.039
Standard deviation	0.139	0.162

Note: Projected drought severity under the RCP 8.5 scenario across the CONUS over the near (2020–2049) and more distant (2030–2059) future, using 1979–2020 as reference period. The drought index is based on SPEI computed at 3–month time scale. A positive value indicates an increasing value of the drought index and intensified future droughts.

Table D.2: *Projected income support payments per operation ($US 2011 prices) by downscaled GCMs, including the multi–model ensemble average (MME), 2030-2059, under the RCP 8.5 scenario, CONUS average*

Downscaled GCMs	Lower 1,5*IQR	25^{th} percentile	Median	75^{th} percentile	upper1,5*IQR
BNU–ESM	-116.7712	13.4284	104.1231	214.8304	356.6244
Bcc–csm1–1	-126.6376	18.0016	117.2638	225.9936	390.2562
Bcc–csm1–1–m	-140.3702	16.9831	115.7427	230.3326	388.8912
CanESM2	-131.1193	7.9418	103.5503	207.6655	348.3503
CCSM4	-99.3247	34.7032	131.5750	251.3458	393.7977
CNRM–CM5	-166.6387	-22.4116	86.7109	199.8914	344.8459
CSIRO–Mk3–6–0	-179.2691	-24.0702	83.6706	193.0364	358.4623
GDFL–ESM2M	-186.9123	-44.5469	58.4372	171.2093	313.6040
GDFL–ESM2G	-205.4363	-24.4946	73.5262	179.8687	340.2081
HadGEM2–CC	-99.5855	54.7562	147.0943	256.5109	407.8241
HadGEM2–ES	-58.2206	94.6860	188.6341	301.1390	454.4175
Inmcm4	-145.5891	0.1371	97.2687	213.5146	370.5537
IPSL–CM5A–LR	-118.6744	25.1484	125.4697	235.3394	382.2408
IPSL–CM5A–MR	-93.6150	39.1114	139.2331	251.1122	407.2486
IPSL–CM5B–LR	-172.3320	-21.3086	79.0066	197.2846	335.6788
MIROC5	-117.0413	21.7421	120.5848	234.5427	394.7268
MIROC5–CHEM	-113.0750	25.5609	125.4080	235.0514	374.1134
MIROC5–ESM	-165.0835	-2.2719	104.1439	223.3413	369.7796
MRI–CGCM3	-198.4592	-43.8263	53.4111	163.3776	317.8471
NorESM1–M	-103.2556	26.6913	128.8525	250.1884	383.3280
MME	-136.8705	9.7981	109.1853	221.7788	371.6399

Note: Projected income support payments for the more distant (2030–2059) future, under the RCP 8.5 scenario. Income support payments per operation and in $US (2011 prices). IQR: interquartile range.